New Approaches for Two-Dimensional DOA Estimation of Coherent and Noncircular Signals with Acoustic Vector-sensor Array

Han Chen

A Thesis
in
The Department
of
Electrical and Computer Engineering

Presented in Partial Fulfillment of the Requirements
for the Degree of Master of Applied Science
(Electrical and Computer Engineering)
Concordia University
Montreal, Quebec, Canada

September 2015

CONCORDIA UNIVERSITY
SCHOOL OF GRADUATE STUDIES

This is to certify that the thesis prepared

By: Han Chen

Entitled: "New Approaches for Two-Dimensional DOA Estimation of Coherent And Noncircular Signals with Acoustic Vector-sensor Array"

and submitted in partial fulfillment of the requirements for the degree of

Master of Applied Science

Complies with the regulations of this University and meets the accepted standards with respect to originality and quality.

Signed by the final examining committee:

_____ Chair
Dr. R. Raut

_____ Examiner, External
Dr. Chun-Yi Su (MIE) To the Program

_____ Examiner
Dr. H. Rivaz

_____ Supervisor
Dr. W-P. Zhu

_____ Supervisor
Dr. M. N. S. Swamy

Approved by: _____
Dr. W. E. Lynch, Chair
Department of Electrical and Computer Engineering

_____20_____ _____
Dr. Amir Asif, Dean
Faculty of Engineering and Computer Science

Abstract

New Approaches for Two-Dimensional DOA Estimation of Coherent and Noncircular Signals with Acoustic Vector-sensor Array

Han Chen

This thesis is mainly concerned with the two-dimensional direction of arrival (2D-DOA) estimation using acoustic vector-sensor array for coherent signals and noncircular signals.

As for coherent signals, the thesis proposes two algorithms, namely, a 2D-DOA estimation algorithm with acoustic vector-sensor array using a single snapshot, and an improved 2D-DOA estimation algorithm of coherent signals. In the first algorithm, only a single snapshot is employed to estimate the 2D-DOA, and the second is an improved algorithm based on the method of Palanisamy et al. Compared to the existing algorithm, the proposed algorithm has the following advantages: (1) lower computational complexity, (2) better estimation performance, and (3) acquiring automatically-paired 2D-DOA estimates.

As for noncircular signals, we propose real-valued space PM and ESPRIT algorithms for 2D-DOA estimation using arbitrarily spaced acoustic vector-sensor array. By exploiting the noncircularity of incoming signals to increase the amount of effective data, the proposed algorithms can provide a better 2D-DOA estimation performance with fewer snapshots, which means a relatively lower sample rate can be used in practical implementations. Compared with the traditional PM and ESPRIT, the proposed algorithms provide better estimation performance while having similar computational complexity. Furthermore, the proposed algorithms are suitable for arbitrary arrays and yield paired azimuth and elevation angle estimates without requiring extra computationally expensive pairing operations.

Acknowledgments

I would like to express my gratitude to my supervisors Dr. Wei-Ping Zhu and Dr. M.N.S. Swamy, for their invaluable help, guidance, and encouragement during my Master's study and research. I thank all the ECE professors and staffs who provided course offering, inspiration and assistance as well as other students who have given me thoughtful ideas and a friendly academic environment.

I send all my love to my family and my girlfriend Ms. Pan for their emotional support and boundless love.

I am grateful to all my friends from Concordia University and Nanjing University of Aeronautics and Astronautics (NUAA), China. They indeed gave me great help and encouragement.

Table of Contents

List of Figures

List of Symbols

$\mathbf{A} \otimes \mathbf{B}$	Kronecker product
$\mathbf{A} \circ \mathbf{B}$	Khatri-Rao matrix product
$\mathbf{A} \odot \mathbf{B}$	Hadamard product
$(.)^*$	Conjugate transpose
$(.)^T$	Transpose
$(.)^H$	Complex conjugate transpose
$(.)^+$	Pseudo-inverse (Moore-Penrose inverse)
$diag\{.\}$	Diagonal matrix with its diagonal elements
$\| \quad \|_F$	Frobenius norm
$angle(.)$	Phase angle
$E[.]$	Expectation
$\mathbf{I}_n$	Identity matrix or unit matrix of size n
$rank\{\bullet\}$	Rank

List of Acronyms

2D	Two Dimensional
AWGN	Additive White Gaussian Noise
BPSK	Binary Phase Shift Keying
CRB	Cramér-Rao Bound
DOA	Direction of Arrival
ESPRIT	Estimation of Signal Parameters via Rotational Invariance Techniques
EVD	Eigenvalue Decomposition
i.i.d	independent and identically distributed
MUSIC	MUltiple SIgnal Classication
PM	Propagator Method
RMSE	Root Mean Square Error
SNR	Signal-to-Noise Ratio
SS	Spatial Smoothing
SVD	Singular Value Decomposition
ULA	Uniform Linear Array

Chapter 1

1 Introduction

1.1 Background

Sensor arrays have been widely applied in many areas like seismology, optical imaging, acoustic imaging, radio astronomy and radar systems. One of the main goals of array signal processing is parameter estimation, especially for the direction of arrival (DOA) estimation. As to scalar sensors like the pressure sensors, the time-difference-of-arrival (TDOA) between scalar sensors of uniform linear arrays (ULAs) is normally used to extract directional information of sources, and thereby estimate the DOA. With the development of sensor technology, a new kind of device, which measures quantities such as velocity and acceleration in addition to pressure, is available. One such device is the acoustic vector sensor. Since an acoustic vector-sensor consists of one pressure hydrophone and three orthogonal velocity hydrophones, it can measure both the pressure and vector components of an acoustic field such as a particle velocity [1]. This advantage allows the acoustic vector sensors to collect more useful information for the signal processing that follows. In the past decades, acoustic vector sensors have attracted a large amount of attentions in the acoustic research community and extensive work has been conducted based on the theory and design of vector sensors. Nowadays, acoustic vector sensors are being widely used for underwater target localizations, acoustic communications and sonar systems.

As mentioned before, an acoustic vector-sensor measures both the pressure and the particle velocity of the acoustic field at a point in space, whereas a traditional pressure sensor can only extract the pressure information. The main advantages of these vector sensors over traditional scalar sensors are their full use of the available acoustic information, better exploitation of beamforming, and hence, their performance in terms of DOA estimation accuracy [2]. Since the measurement model for acoustic vector sensor array [1] was developed in 1994, a great deal of research on DOA estimation of incoming signals has been performed, leading to many DOA estimation techniques [4-18]. However, most of these methods suffer serious degradation when the incident signals are coherent, as in some practical scenarios, due to multipath propagation. In addition to coherent signals, noncircular signals are also widely used in underwater

communications [24]. By exploiting the noncircularity of the signals, a better DOA estimation performance can be achieved, but not much research work of exploiting the noncircularity of signals to estimate 2D-DOA with acoustic vector-sensor array has been reported.

1.2 Literature Review

Acoustic vector sensor model was first introduced to the signal processing community in [3]. Since then, more and more advanced DOA estimation approaches with acoustic vector-sensor array have been presented [4-18]. To some extent, these approaches can be divided into two classes: parametric methods and spatial spectral-based methods. With regard to the parametric methods, they need global searches for all possible parameters which apparently lead to high computational complexity, and hence are difficult to be implemented in practical situations. Spatial spectral-based methods estimate the DOAs by finding the extremes of the spatial spectral functions. This class of methods can also be divided into two subclasses. One is combining spatial spectral-methods with traditional beamforming techniques; the estimation performance of these methods, however, is strictly limited to the amount of array sensors. The authors of [4] proposed a maximum likelihood-based DOA estimator with acoustic vector-sensor array in the presence of an isotropic noise field. Traditional beamforming and Capon method for DOA estimation were extended to vector-sensor arrays in [5], and the authors therein also found that the vector sensors' directional sensitivity removes all bearing ambiguities and even simple structures such as linear arrays can determine both azimuth and elevation angles, and spatially undersampled regularly spaced arrays may be employed to increase aperture and, hence, improve the performance. The other one is combining spatial spectral-methods with the super-resolution DOA estimation techniques such as MUSIC [6][7]. The estimation performance of this subclass of methods is no longer limited to the size of sensors array and hence gets greatly improved. A novel blind MUSIC-based source localization algorithm applicable to an arbitrarily spaced acoustic vector-sensor array is introduced in [6], which uses ESPRIT to self-generate coarse estimates of the DOA to start off its MUSIC-based iterative search with no a priori source information. The method in [7] uses polynomial rooting to estimate DOA with acoustic vector sensors uniformly spaced in an L-shaped array configuration. This algorithm can also be used with nonuniform nonlinear arrays via the "virtual array interpolation" method. Although these

MUSIC-based methods have excellent DOA estimation performance in terms of accuracy, they normally require iterative 2D searches, which is not computationally effective.

To avoid the enormous complexity of 2D search, some researchers have introduced classic ESPRIT to the DOA estimation of acoustic vector sensor array and proposed several improved methods [9][10]. Benefited from the high-resolution of classic ESPRIT, these novel ESPRIT based methods also have remarkable estimation accuracy. The authors of [9] introduced a novel ESPRIT-based closed-form source localization algorithm applicable to arbitrarily spaced acoustic vector sensors, whose locations need not be known. A novel ESPRIT-based 2D DOA estimation scheme using a uniform rectangular acoustic vector-sensor array was proposed in [10], which enlarges the array aperture, but needs no additional sensors, requires no nonuniform interelement spacing, and altogether avoids the direction-cosine ambiguity that commonly arises when interelement spacing exceeds the Nyquist half-wavelength upper limit.

The subspace-based methods, such as ESPRIT and MUSIC, however, require eigen-value decomposition (EVD) of the cross correlation matrix and singular value decomposition (SVD) of the received data to obtain signal subspace or noise subspace, which still brings in fairly heavy computational burden. A computationally simple 2D-DOA finding algorithm in spatially correlated noise fields using two-far-separated subarray geometry was presented in [8]. The authors firstly defined a cross matrix to eliminate the effect of the spatially correlated noise. Then the propagator method (PM) was used to estimate the steering vectors of acoustic vector sensors. Finally, automatically-paired azimuth and elevation angle estimates were derived in a closed form. The algorithm in [8] requires no eigen decomposition into signal or noise subspaces nor any 2D iterative searching and hence the algorithm has low computational complexity. The authors of [18] also presented a PM based algorithm employing only one acoustic vector sensor to estimate DOAs. Since they don't need global searches, EVD or SVD, the computational complexity of these PM-based algorithms are significantly lower than that of ESPRIT or MUSIC-based algorithms.

The DOA estimation algorithms mentioned above have been proven to be accurate and efficient in dealing with the DOA estimation problem of incoherent sources. But, when the sources are coherent or partially coherent, for example in multipath propagation situation, the

performance of these algorithms will degrade significantly because the rank of the source signal covariance matrix becomes less than the number of incident signals. To overcome this, some decorrelated methods using scale sensors were proposed, such as the spatial smoothing techniques [19-21], EVD smoothing techniques [22][23], the computationally efficient subspace-based method without eigen-decomposition (SUMWE) [42] as well as others. These scale sensors based methods, however, work well only for certain array structures, for example, uniform linear arrays. With respect to vector-sensor, the authors of [29] proposed a computationally simple 2-D direction finding algorithm using a uniform linear array of vector hydrophones, which can be regarded as an improvement of SUMWE algorithm. The authors of [30] presented two methods for estimating 2-D DOA of coherent signals using an L-shaped array of acoustic vector sensors, but extra pair matching is required in these methods.

Noncircular signals, such as the binary phase shift keying (BPSK) modulated signals, are found to be bandwidth efficient in underwater communications [24]. A signal $s(t)$ is said to be noncircular if its complementary covariance $\mathbf{C} = E[\mathbf{x}\mathbf{x}^T] \neq \mathbf{O}$. In other words, noncircular signals have nonvanishing conjugate correlation. This statistical redundancy can be used to increase the effective data and hereby makes it possible to achieve a better 2D-DOA estimation performance. However, most of the existing algorithms for 2D-DOA estimation using acoustic vector sensor array mentioned above do not utilize the noncircularity of the signals and little research work of exploiting the noncircularity of signals to estimate 2D-DOA with acoustic vector-sensor array has been reported. Some 2D-DOA estimation algorithms for noncircular signals using scalar sensor array are available in [25][26], but array geometries applied to these methods are strictly limited. The authors of [25] presented a polynomial rooting technique-based direction finding algorithm for noncircular sources, and due to the noncircularity characteristics of the impinging sources, this method is able to handle more sources than sensors. In the meantime, the use of polynomial rooting instead of a searching technique, however, limits the method to linear uniformly spaced arrays. Haardt. et al. proposed a real-valued implementation of 2D Unitary ESPRIT for noncircular sources in [26], but uniform rectangular arrays are required, which may be difficult to realize in practical situations.

1.3 Thesis Outline

The organization of the thesis is presented as follows.

Chapter 2 discusses the fundamentals of array signal processing using acoustic vector sensor array, including the acoustic vector sensor measurements, the received noise model, three array structures that will be used in the later chapters, and Cramer-Rao bound (CRB).

In Chapter 3, we propose two 2D-DOA estimation methods for coherent incident sources using acoustic vector-sensor array. In the first algorithm, only a single snapshot is employed to estimate the 2D-DOA, and the second is an improved algorithm based on that of Palanisamy et al [30]. Compared to the PKS algorithm, this proposed algorithm has the following advantages: (1) lower computational complexity, (2) better estimation performance, and (3) acquiring automatically-paired 2D-DOA estimates.

In Chapter 4, real-valued space PM and ESPRIT algorithms for 2D-DOA estimation of noncircular signals using arbitrarily spaced acoustic vector sensor array are proposed. By exploiting the noncircularity of the incoming signals to increase the amount of effective data, the proposed algorithms can provide better 2D-DOA estimation performance with fewer snapshots, which means a relatively lower sample rate can be used in practical implementations. Compared with the traditional PM and ESPRIT, the proposed algorithms provide better estimation performance, with a similar computational complexity. Furthermore, the proposed algorithms are suitable for arbitrary array and yield paired azimuth and elevation angle estimates without requiring extra computationally-expensive pairing operations.

Finally, Chapter 5 contains conclusions and provides some directions for future work.

Chapter 2

2 Fundamentals of Array Signal Processing Using Acoustic Vector Sensor Array

This chapter mainly introduces the fundamentals of array signal processing using acoustic vector sensor array, which include the acoustic vector sensor measurements, the noise model and three array structures used in the later chapters.

2.1 Acoustic Vector Sensor Measurement

In this thesis, the acoustic wave is assumed to be plane at the sensor. Let $\mathbf{u}_k$ denote the unit vector at the sensor pointing towards the *k*th source, which is

$$\mathbf{u}_k = \begin{bmatrix} \cos\phi_k \cos\varphi_k \\ \sin\phi_k \cos\varphi_k \\ \sin\varphi_k \end{bmatrix} \tag{2.1}$$

where ϕ_k and φ_k represent the azimuth and elevation angles, respectively, with $0 \le \phi_k < 360^0$ and $0 \le \varphi_k < 90^0$, as shown in Figure 2.1

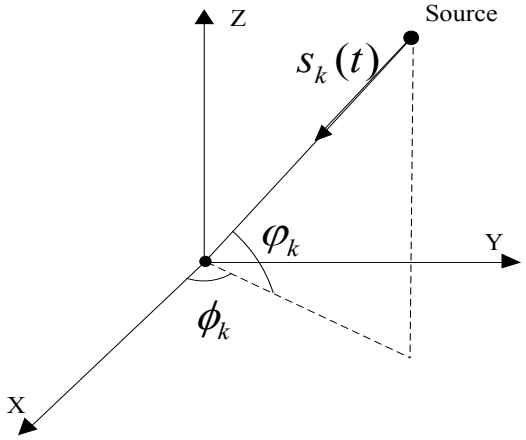

Figure 2.1 2D Direction of arrival

The acoustic pressure component of the measurement is

$$x_p(t) = s(t) + n_p(t) \tag{2.2}$$

where $s(t)$ denotes the acoustic pressure of the signal at time t, and $n_p(t)$ is the corresponding noise. Similarly, the velocity component of the measurement is

$$\mathbf{x}_v(t) = s(t) \cdot \mathbf{u} + \mathbf{n}_v(t) \tag{2.3}$$

Combining (2.2) and (2.3), we get the complete measurement of a single acoustic vector sensor, denoted as

$$\begin{bmatrix} x_p(t) \\ \mathbf{x}_v(t) \end{bmatrix} = \begin{bmatrix} 1 \\ \mathbf{u} \end{bmatrix} s(t) + \begin{bmatrix} n_p(t) \\ \mathbf{n}_v(t) \end{bmatrix} \tag{2.4}$$

Now we consider a total of *K* independent acoustic waves impinging on an arbitrarily spaced array containing *M* acoustic vector sensors. To extend the model (2.4) to this scenario, let $\mathbf{x}_{pv}(t)$ and $\mathbf{n}_{pv}(t)$ be the *4M×1* dimensional pressure-velocity measurement and noise vectors. Then, the output of the array is given by

$$\mathbf{x}_{pv}(t) = \sum_{k=1}^{K} \mathbf{a}_k \otimes \begin{bmatrix} 1 \\ \mathbf{u}_k \end{bmatrix} s_k(t) + \mathbf{n}_{pv}(t) \tag{2.5}$$

where $\mathbf{a}_k$ is the *k*th column of steering matrix $\mathbf{A}$, whose (j,k) element is represented as

$$\mathbf{A}(j,k) = e^{-i\omega_c \tau_{jk}} \tag{2.6}$$

where τ_{jk} is the differential time delay of the *k*th wave between the reference and the *j*th sensor, and ω_c is the frequency of the wave.

2.2 Noise Model

We assume that the noise is independent of the source, and noise is additive independent and identically distributed *(i.i.d.)* Gaussian with zero mean and variance σ^2. The covariances of the noise vector $\mathbf{n}(t)$ satisfies

$$E\{\mathbf{n}(t_1)\mathbf{n}^{\mathrm{H}}(t_2)\}=\sigma^2\mathbf{I}\delta_{t_1,t_2} \tag{2.7}$$

$$E\{\mathbf{n}(t_1)\mathbf{n}^{T}(t_2)\}=\mathbf{O} \tag{2.8}$$

where $\mathbf{n}(t_1)$ and $\mathbf{n}(t_2)$ represent the noise output at time t_1 and t_2, respectively, $\mathbf{I}$ and $\mathbf{O}$ indicate the identity matrix and the null matrix. Here δ_{t_1,t_2} is the Dirac function.

2.3 Array Structures

In this section, we mainly discuss three array structures which will be used in this thesis, namely, uniform linear array, L-shaped array and arbitrarily spaced array.

2.3.1 Uniform Linear Array

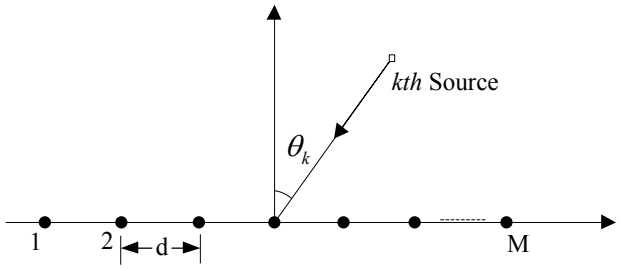

Figure 2.2 Uniform linear array

As shown in Figure 2.2, a uniform linear array arranges *M* sensor elements along a line in space with a uniform spacing *d*. We consider *K* independent sources with wavelength λ and DOA θ_k (k=1,2,…,K) impinging on this array; then, the steering vector of kth source is given by

$$\mathbf{a}(\theta_k)=\begin{bmatrix}1 & \exp(-j2\pi d\sin\theta_k/\lambda) & \cdots & \exp(-j2\pi(M-1)d\sin\theta_k/\lambda)\end{bmatrix}^T \tag{2.9}$$

We get the steering matrix of all *K* sources as

$$\mathbf{A}=[\mathbf{a}(\theta_1),\mathbf{a}(\theta_2),....,\mathbf{a}(\theta_K)]$$

$$= \begin{bmatrix} 1 & 1 & \cdots & 1 \\ e^{-j2\pi d \sin\theta_1/\lambda} & e^{-j2\pi d \sin\theta_2/\lambda} & \cdots & e^{-j2\pi d \sin\theta_K/\lambda} \\ \vdots & \vdots & \vdots & \vdots \\ e^{-j2\pi(M-1)d \sin\theta_1/\lambda} & e^{-j2\pi(M-1)d \sin\theta_2/\lambda} & \cdots & e^{-j2\pi(M-1)d \sin\theta_K/\lambda} \end{bmatrix} \tag{2.10}$$

where (2.10) is a Vandermonde matrix. It should be mentioned that a linear array of traditional scalar sensors can only be used to estimate 1D DOA, but the uniform linear array of vector sensors can determine both azimuth and elevation angles because of its directional sensitivity.

2.3.2 L-shaped Array

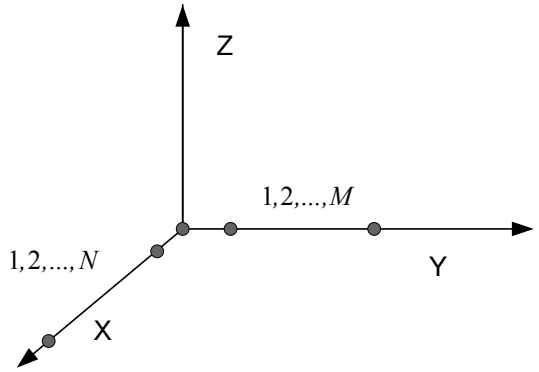

Figure 2.3 L-shaped array

Consider that an L-shaped array contains (*M*+*N*-1) sensor elements, and the sub-array along the x-direction consists of *N* sensor elements with uniform spacing d_x, and that along the y-direction consists of *M* sensor elements with uniform spacing d_y. These two sub-arrays have a common element at the origin, as shown in Figure 2.3. In most cases, $d_x = d_y = d$. We consider *K* independent sources impinging on this array with 2D-DOA (ϕ_k, φ_k), where ϕ_k, φ_k denote the azimuth and elevation angles of the *k*th source. The steering vector of the *k*th source of x-direction sensors and y-direction sensors can be denoted as

$$\mathbf{a}_x(\varphi_k, \phi_k) = \begin{bmatrix} 1 \\ \exp(-j2\pi d \cos\phi_k \sin\varphi_k / \lambda) \\ \vdots \\ \exp(-j2\pi(N-1)d \cos\phi_k \sin\varphi_k / \lambda) \end{bmatrix} \tag{2.11}$$

$$\mathbf{a}_y(\varphi_k,\phi_k)=\begin{bmatrix}1\\ \exp(-j2\pi d\sin\phi_k\sin\varphi_k/\lambda)\\ \vdots\\ \exp(-j2\pi(M-1)d\sin\phi_k\sin\varphi_k/\lambda)\end{bmatrix} \tag{2.12}$$

Hence the steering matrix of x-direction sensors corresponding to all K sources is given by

$$\mathbf{A}_x=[\mathbf{a}_x(\varphi_1,\phi_1),\mathbf{a}_x(\varphi_2,\phi_2),\cdots,\mathbf{a}_x(\varphi_K,\phi_K)]$$

$$=\begin{bmatrix}1 & 1 & \cdots & 1\\ \exp(-j2\pi d\cos\phi_1\sin\varphi_1/\lambda) & \exp(-j2\pi d\cos\phi_2\sin\varphi_2/\lambda) & \cdots & \exp(-j2\pi d\cos\phi_K\sin\varphi_K/\lambda)\\ \vdots & \vdots & \ddots & \vdots\\ \exp(-j2\pi d(N-1)\cos\phi_1\sin\varphi_1/\lambda) & \exp(-j2\pi d(N-1)\cos\phi_2\sin\varphi_2/\lambda) & \cdots & \exp(-j2\pi d(N-1)\cos\phi_K\sin\varphi_K/\lambda)\end{bmatrix} \tag{2.13}$$

Similarly, the steering matrix of y-direction sensors can be denoted as

$$\mathbf{A}_y=[\mathbf{a}_y(\varphi_1,\phi_1),\mathbf{a}_y(\varphi_2,\phi_2),\cdots,\mathbf{a}_y(\varphi_K,\phi_K)]$$

$$=\begin{bmatrix}1 & 1 & \cdots & 1\\ \exp(-j2\pi d\sin\varphi_1\sin\phi_1/\lambda) & \exp(-j2\pi d\sin\varphi_2\sin\phi_2/\lambda) & \cdots & \exp(-j2\pi d\sin\varphi_K\sin\phi_K/\lambda)\\ \vdots & \vdots & \ddots & \vdots\\ \exp(-j2\pi d(M-1)\sin\varphi_1\sin\phi_1/\lambda) & \exp(-j2\pi d(M-1)\sin\varphi_2\sin\phi_2/\lambda) & \cdots & \exp(-j2\pi d(M-1)\sin\varphi_K\sin\phi_K/\lambda)\end{bmatrix} \tag{2.14}$$

There has been a growing interest in developing 2D-DOA estimates using the L-shaped array for better estimation performance and without encountering the pair-matching problem. Concerning the L-shaped array of scale sensors, Tayem and Kwon [43] proposed a method for estimating 2D-DOA in the presence of uncorrelated or partially correlated signals exploiting the L-shaped array structure. Kikuchi et al. [44] developed an automatic pair-matching method for DOA estimation using the cross-correlation matrix. Gu et al. [45] developed an effective 2D-DOA estimation method for narrowband coherent signals using L-shaped arrays. Palanisamy et al. [30] developed an effective 2D-DOA estimation method for narrowband coherent signals using an L-shaped acoustic vector sensor array. Based on this, we propose an improved algorithm in Section

3.3, which has lower computational complexity, better estimation performance as well as acquiring automatically-paired 2D-DOA estimates.

2.3.3 Arbitrarily Spaced Array

We consider M sensor elements arbitrarily placed in the space and the mth sensor is located at $\mathbf{l}_m = (x_m, y_m, z_m)$, and K independent sources impinge on this array. Then the steering vector of the kth source can be shown to be

$$\mathbf{a}(\varphi_k, \phi_k) = \begin{bmatrix} 1 \\ \exp[-j2\pi(x_1 \sin\varphi_k \cos\phi_k + y_1 \sin\varphi_k \sin\phi_k + z_1 \cos\varphi_k)/\lambda] \\ \vdots \\ \exp[-j2\pi(x_{M-1} \sin\varphi_k \cos\phi_k + y_{M-1} \sin\varphi_k \sin\phi_k + z_{M-1} \cos\varphi_k)/\lambda] \end{bmatrix} \tag{2.15}$$

where λ is the wavelength. Hence the steering matrix is given by

$$\mathbf{A} = [\mathbf{a}(\varphi_1, \phi_1), \mathbf{a}(\varphi_2, \phi_2), \cdots, \mathbf{a}(\varphi_K, \phi_K)] \tag{2.16}$$

In Chapter 4, we proposed real-valued space PM and ESPRIT algorithms for 2D-DOA estimation of noncircular signals using arbitrarily spaced acoustic vector sensor array. Both of the proposed algorithms do not require any a priori knowledge of the location of any of the vector sensors, because the propagator of the PM and the invariant factors of the ESPRIT, which are used to estimate 2D-DOA, depend only on the source parameters.

2.4 Cramer-Rao Bound

The Cramer-Rao Bound (CRB) is a lower bound on the variance of all unbiased estimators of some parameter or set of parameters. Consider the problem of finding the K sources parameter vector $\boldsymbol{\theta} = [\phi_1, \varphi_1, \phi_2, \varphi_2, ..., \phi_K, \varphi_K]$, where ϕ_k and φ_k stand for the azimuth angle and the elevation angle of the kth source, respectively, in the following discrete-time acoustic vector-sensor array model associated with M vector sensors

$$\mathbf{x}(t) = \mathbf{A}(\boldsymbol{\theta})\mathbf{s}(t) + \mathbf{n}(t) \qquad t=1,2,\ldots,L \tag{2.17}$$

where $\mathbf{x}(t)$ is the output of the array at time t, $\mathbf{s}(t)$ is the source signals, and $\mathbf{n}(t)$ is an additive noise. We assume that the source signal sequence $\{\mathbf{x}(1), \mathbf{x}(2), ..., \mathbf{x}(L)\}$ is an independent identically distributed (i.i.d.) Gaussian process with zero mean and

$$\begin{aligned} E[\mathbf{x}(t)\mathbf{x}^H(s)] &= \mathbf{P}\delta_{t,s} \\ E[\mathbf{x}(t)\mathbf{x}^T(s)] &= \mathbf{O} \end{aligned} \qquad \text{for all } t \text{ and } s \tag{2.18}$$

We also assume that the matrix $\mathbf{A}(\boldsymbol{\theta})$ has full rank. For notational simplicity we will omit the explicit dependence on $\boldsymbol{\theta}$ and t. Considering the estimation of $\boldsymbol{\theta}$ in the model (2.17) under the above assumptions and with $\boldsymbol{\theta}$, $\mathbf{P}$ and the noise variance σ^2 unknown, Theorem 3.1 of [1] gives a compact matrix expression for the CRB on the DOA parameters with an acoustic vector-sensor array, namely,

$$CRB = \frac{\sigma^2}{2L}\left\{\mathrm{Re}\left[\left(\mathbf{D}^H \Pi_{\mathbf{A}}^{\perp} \mathbf{D}\right) \odot \hat{\mathbf{P}}^T\right]\right\}^{-1} \tag{2.19}$$

where $\odot$ is the Hadamard (elementwise) product,

$$\mathbf{D} = [\mathbf{d}_{1\varphi}, \mathbf{d}_{2\varphi}, ..., \mathbf{d}_{K\varphi}, \mathbf{d}_{1\phi}, \mathbf{d}_{2\phi}, ..., \mathbf{d}_{K\phi}] \text{ with } \mathbf{d}_{k\varphi} = \frac{\partial \mathbf{A}}{\partial \varphi_k} \text{ and } \mathbf{d}_{k\phi} = \frac{\partial \mathbf{A}}{\partial \phi_k} \tag{2.20}$$

$$\hat{\boldsymbol{P}} = \begin{bmatrix} \hat{\boldsymbol{P}}_s & \hat{\boldsymbol{P}}_s \\ \hat{\boldsymbol{P}}_s & \hat{\boldsymbol{P}}_s \end{bmatrix} \text{ with } \hat{\boldsymbol{P}}_s = \frac{1}{L}\sum_{t=1}^{L} \boldsymbol{x}(t)\boldsymbol{x}^H(t) \tag{2.21}$$

$$\Pi_{\mathbf{A}}^{\perp} = \mathbf{I}_{4M} - \mathbf{A}(\mathbf{A}^H\mathbf{A})^{-1}\mathbf{A}^H \tag{2.22}$$

and $\mathbf{I}_{4M}$ is the identity matrix of size $4M$. Furthermore, the CRB in (2.19) remains the same independently of whether σ^2 is known or unknown. For the details of the expression, see Appendix C of [41].

2.5 Summary

We have discussed in this chapter some fundamentals of array signal processing using acoustic vector sensor array, including the acoustic vector sensor measurements, the received noise model

and three array structures that will be used in the later chapters of this thesis. The model and assumptions introduced in this chapter applies to the entire thesis.

Chapter 3

3 2D-DOA Estimation of Coherent Sources with Acoustic Vector-Sensor Array

3.1 Introduction

This chapter deals with the 2D-DOA estimation problem of coherent sources using acoustic vector-sensor array. Some vector sensors-based high-resolution DOA estimation algorithms, such as MUSIC [6][7] and ESPRIT[9][10], have been proven to be accurate and efficient in dealing with the DOA estimation problem of incoherent sources. But, when the sources are coherent or partially coherent, for example in multipath propagation situation, the performance of these algorithms will degrade significantly because the rank of the source signal covariance matrix becomes less than the number of incident signals. To overcome this, some decorrelated methods, such as spatial smoothing techniques [19-21], EVD smoothing techniques [22][23], and SUMWE [42], have been proposed. However, certain array structures, for example ULA, are required for these scale sensors-based methods. The author in [29] proposed a SUMWE-based computationally simple 2D direction finding algorithm using a ULA of vector hydrophones. The authors of [30] presented two methods for estimating 2D-DOA of coherent signals using an L-shaped array of acoustic vector sensors, but extra pair matching is required in these methods.

In this chapter, we propose two 2D-DOA estimation methods for coherent incident sources using acoustic vector-sensor array. In the first algorithm, only a single snapshot is employed to estimate the 2D-DOA, while the second is an improved algorithm based on the method of Palanisamy et al [30]. Compared to the algorithm of [30], the proposed algorithm has the following advantages: (1) lower computational complexity, (2) better estimation performance, and (3) acquiring automatically-paired 2D-DOA estimates.

3.2 2D-DOA Estimation of Coherent Sources with Acoustic Vector-Sensor Array Using a Single Snapshot

Compared with subspace-based methods, such as MUSIC and ESPRIT, the PM has lower computational complexity. However, only in high-snapshots situation, can the PM algorithm yield a better estimation performance. Besides, all of these algorithms mentioned above cannot

work for coherent sources. In this section, we combine PM with Toeplitz Hermitian matrix representation, and propose an improved algorithm, which works well in the case of coherent signals and a single snapshot. Furthermore, the proposed method can achieve automatically-paired 2D angle estimates. Simulation results are provided showing that the proposed method has a better performance and less computational complexity than spatial smoothing methods do.

3.2.1 Data Model

We consider that a total of *K* narrowband plane waves impinge on a uniform linear array containing *M=2N+1* acoustic vector sensors, as shown in Figure 3.1. The reference acoustic vector sensor is located at the origin of coordinates, and the distance between two adjacent acoustic vector sensors is *d*. We consider that the signals are in the far-field and the noise is independent of the source, and noise is additive *i.i.d.* Gaussian. Let the *k*th signal arrive from direction (ϕ_k, φ_k), where ϕ_k and φ_k stand for the azimuth angle and the elevation angle, respectively. Let $\boldsymbol{\theta}_k = [\phi_k, \varphi_k]^T$ be the 2D-DOA of the *k*th source. In the scenario of free-spacing, the noise-free output of an acoustic vector sensor at $\mathbf{x}_m$ can be shown to be [6][7]

$$\mathbf{x}_m(t) = \sum_{k=1}^{K} \begin{bmatrix} 1 \\ \mathbf{u}_k \end{bmatrix}^T e^{-j2\pi\tau_{mk}} s_k(t)$$

where $s_k(t)$ is the transmit signal of the *k*th source, τ_{mk} is the differential time delay of the *k*th wave between the origin and the *m*th sensor, 1 and $\mathbf{u}_k$ are the pressure component and the velocity components, respectively. Here $\mathbf{u}_k$ is given by

$$\mathbf{u}_k = \begin{bmatrix} \cos\phi_k \cos\varphi_k \\ \sin\phi_k \cos\varphi_k \\ \sin\varphi_k \end{bmatrix} = \begin{bmatrix} \alpha(\boldsymbol{\theta}_k) \\ \beta(\boldsymbol{\theta}_k) \\ \gamma(\boldsymbol{\theta}_k) \end{bmatrix}$$

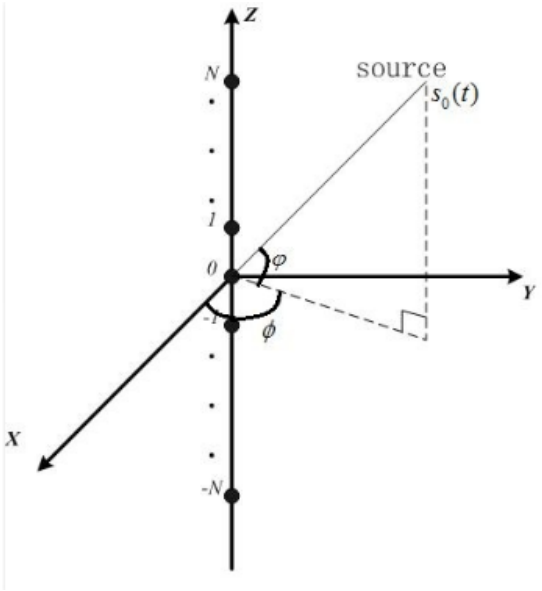

Figure 3.1 The structure of array

According to the symmetry of the array containing *M* acoustic vector sensors, the output can be expressed as

$$\mathbf{X}(\mathrm{t}) = \begin{bmatrix} \mathbf{x}_{-N}(t) \\ \vdots \\ \mathbf{x}_0(t) \\ \vdots \\ \mathbf{x}_N(t) \end{bmatrix} = \mathbf{A}(\boldsymbol{\theta})\mathbf{S}(\mathrm{t}) + \mathbf{N}(\mathrm{t})$$

where $\mathbf{S}(\mathrm{t})$ contains *K* source signals, $\mathbf{N}(\mathrm{t})$ is the received additive white Gaussian noise (AWGN) vector with zero mean and covariance matrix $\sigma^2\mathbf{I}_{4M}$.

$$\mathbf{A}(\boldsymbol{\theta}) = \left[\mathbf{a}(\varphi_1)\otimes\mathbf{h}_1 \quad \mathbf{a}(\varphi_2)\otimes\mathbf{h}_2 \quad \cdots \quad \mathbf{a}(\varphi_K)\otimes\mathbf{h}_K\right]$$

where $\mathbf{a}(\varphi_k) = [\exp(i2\pi Nd\sin\varphi_k/\lambda),\cdots,\exp(i2\pi d\sin\varphi_k/\lambda),1,\exp(-i2\pi d\sin\varphi_k/\lambda),\cdots,\exp(-i2\pi Nd\sin\varphi_k/\lambda)]^T$, and $\mathbf{a}(\varphi_k)$ is the $M \times 1$ steering vector of an acoustic pressure sensor array with the same geometry as the acoustic vector sensor array for the *k*th signal, and $\mathbf{h}_k = [1, \mathbf{u}_k^T]^T$ is the bearing vector of the *k*th source.

3.2.2 DOA Estimation Using a Single Snapshot

3.2.2.1 Data Representation

The proposed method gets rid of the negative effects of coherent incident signals by constructing the Toeplitz Hermitian data matrix. First, the snapshot is set to be unity, and a Toeplitz data matrix $\mathbf{Y}$ is defined as

$$\mathbf{Y} = \begin{bmatrix} \mathbf{x}_0 & \mathbf{x}_{-1} & \mathbf{x}_{-2} & \cdots & \mathbf{x}_{-N} \\ \mathbf{x}_1 & \mathbf{x}_0 & \mathbf{x}_{-1} & \cdots & \mathbf{x}_{-(N-1)} \\ \mathbf{x}_2 & \mathbf{x}_1 & \mathbf{x}_0 & \cdots & \mathbf{x}_{-(N-2)} \\ \vdots & \vdots & \vdots & \ddots & \vdots \\ \mathbf{x}_N & \mathbf{x}_{N-1} & \mathbf{x}_{N-2} & \cdots & \mathbf{x}_0 \end{bmatrix} \tag{3.1}$$

where $\mathbf{Y} \in \mathbb{C}^{4(N+1)\times(N+1)}$, and $\mathbf{x}_m(-N \le m \le N)$ is a component of the output matrix $\mathbf{X}(\mathrm{t})$. $\mathbf{Y}$ can also be expressed as

$$\mathbf{Y} = \left[\mathbf{B}(\boldsymbol{\theta})\mathbf{S}, \mathbf{B}(\boldsymbol{\theta})\boldsymbol{\Phi}\mathbf{S}\cdots\mathbf{B}(\boldsymbol{\theta})\boldsymbol{\Phi}^N\mathbf{S}\right] + \mathbf{N}(t)$$

where $\mathbf{B}(\boldsymbol{\theta}) = \left[\mathbf{b}(\varphi_1)\otimes\mathbf{h}_1 \quad \mathbf{b}(\varphi_2)\otimes\mathbf{h}_2 \quad \cdots \quad \mathbf{b}(\varphi_K)\otimes\mathbf{h}_K\right]$, $\mathbf{b}(\varphi_k) = [1, \exp(-i2\pi d\sin\varphi_k/\lambda), \cdots, \exp(-i2\pi Nd\sin\varphi_k/\lambda)]^T$ and $\boldsymbol{\Phi} = diag\{\exp(-i2\pi d\sin\varphi_1/\lambda), \cdots, \exp(-i2\pi d\sin\varphi_K/\lambda)\}$.

Then we construct a Toeplitz Hermitian matrix via

$$\mathbf{Y}_1 = \mathbf{J}_1\mathbf{Y}^*\mathbf{J}_2 \tag{3.2.a}$$

$$\mathbf{Z} = (\mathbf{Y} + \mathbf{Y}_1)/2 \tag{3.2.b}$$

where $\mathbf{J}_1 \in \mathbb{Z}^{4(N+1)\times 4(N+1)}$ can be obtained by

$$\mathbf{J}_1 = \begin{bmatrix} \mathbf{0}_4 & \mathbf{0}_4 & \ldots & \mathbf{0}_4 & \mathbf{I}_4 \\ \mathbf{0}_4 & \iddots & \iddots & \mathbf{I}_4 & \mathbf{0}_4 \\ \vdots & \iddots & \iddots & \iddots & \vdots \\ \mathbf{0}_4 & \mathbf{I}_4 & \iddots & \iddots & \mathbf{0}_4 \\ \mathbf{I}_4 & \mathbf{0}_4 & \ldots & \mathbf{0}_4 & \mathbf{0}_4 \end{bmatrix}$$

where $\mathbf{0}_4$ is a *4×4* zero matrix and $\mathbf{I}_4$ is a *4×4* identity matrix, while $\mathbf{J}_2 \in \mathbb{Z}^{(N+1)\times(N+1)}$ can be expressed as

$$\mathbf{J}_2 = \begin{bmatrix} 0 & 0 & \dots & 0 & 1 \\ 0 & \iddots & \iddots & 1 & 0 \\ \vdots & \iddots & \iddots & \iddots & \vdots \\ 0 & 1 & \iddots & \iddots & 0 \\ 1 & 0 & \dots & 0 & 0 \end{bmatrix}$$

By transforming the matrix $\mathbf{Z}$ using the exchange matrix $\mathbf{J}$ to bring the pressure components and the velocity components of the acoustic vector sensors together, which is a necessary step of getting estimated angles in the following subsection, obtain a new transformed matrix $\tilde{\mathbf{Z}}$ as given by

$$\tilde{\mathbf{Z}} = \mathbf{J}^T \mathbf{Z} \tag{3.3}$$

where $\mathbf{J} = [\mathbf{e}_1, \mathbf{e}_2, \mathbf{e}_3, \mathbf{e}_4]$ is a $4(N+1)\times 4(N+1)$ matrix, $\mathbf{e}_i = [e_i, e_{i+4}, e_{i+8}, ..., e_{i+4N}]$ for i=1,2,3,4, and e_i is the $4(N+1)\times 1$ unit vector whose ith component is unity and all others are zero.

3.2.2.2 DOA Estimation

Here we use PM to estimate the 2D-DOAs. Define $\tilde{\mathbf{B}}(\varphi)$ as

$$\tilde{\mathbf{B}}(\varphi) = \mathbf{J}^T \mathbf{B}(\varphi) = \begin{bmatrix} \mathbf{B}_1 \\ \mathbf{B}_2 \\ \mathbf{B}_3 \\ \mathbf{B}_4 \end{bmatrix} = \begin{bmatrix} \mathbf{B}_1 \\ \mathbf{B}_1\boldsymbol{\alpha} \\ \mathbf{B}_1\boldsymbol{\beta} \\ \mathbf{B}_1\boldsymbol{\gamma} \end{bmatrix} \tag{3.4}$$

where $\boldsymbol{\alpha} = diag\{\alpha(\boldsymbol{\theta}_1), \alpha(\boldsymbol{\theta}_2), ..., \alpha(\boldsymbol{\theta}_K)\}$, $\boldsymbol{\beta} = diag\{\beta(\boldsymbol{\theta}_1), \beta(\boldsymbol{\theta}_2), ..., \beta(\boldsymbol{\theta}_K)\}$, and $\boldsymbol{\gamma} = diag\{\gamma(\boldsymbol{\theta}_1), \gamma(\boldsymbol{\theta}_2), ..., \gamma(\boldsymbol{\theta}_K)\}$. Partition the matrix $\tilde{\mathbf{B}}(\varphi)$ as

$$\tilde{\mathbf{B}}(\varphi) = \begin{bmatrix} \tilde{\boldsymbol{B}}_1(\varphi) \\ \tilde{\boldsymbol{B}}_2(\varphi) \end{bmatrix} \tag{3.5}$$

where $\tilde{\boldsymbol{B}}_1(\varphi)$ is a $K\times K$ nonsingular matrix, and $\tilde{\boldsymbol{B}}_2(\varphi)$ is a $[4(N+1)-K]\times K$ matrix. Then $\tilde{\boldsymbol{B}}_2(\varphi)$ is a linear transformation of $\tilde{\boldsymbol{B}}_1(\varphi)$,

$$\tilde{\mathbf{B}}_2(\theta) = \mathbf{P}^H \tilde{\mathbf{B}}_1(\theta) \tag{3.6}$$

where $\mathbf{P} \in \mathbb{C}^{K\times[4(N+1)-K]}$ is the propagator matrix. We define $\mathbf{P}_E \in \begin{bmatrix} \mathbf{I}_{K\times K} \\ \mathbf{P}^H \end{bmatrix}$, and then have

$$\tilde{\mathbf{B}}(\varphi) = \mathbf{P}_E \tilde{\boldsymbol{B}}_1(\varphi) \tag{3.7}$$

The propagator $\mathbf{P}$ can be obtained from $\tilde{\mathbf{Z}}$, which we partition as

$$\tilde{\mathbf{Z}} = \begin{bmatrix} \tilde{\mathbf{Z}}_1 \\ \tilde{\mathbf{Z}}_2 \end{bmatrix} \tag{3.8}$$

where $\tilde{\mathbf{Z}}_1$ is a $K\times K$ nonsingular matrix, and $\tilde{\mathbf{Z}}_2$ is a $[4(N+1)-K]\times K$ matrix. In the noise-free case,

$$\tilde{\mathbf{Z}}_2 = \mathbf{P}^H \tilde{\mathbf{Z}}_1 \tag{3.9}$$

Actually, there is always noise, and the propagator matrix can be estimated by the follow minimization problem

$$J_{csm}(\mathbf{P}) = \left\| \tilde{\mathbf{Z}}_2 - \mathbf{P}^H \tilde{\mathbf{Z}}_1 \right\|_{\mathrm{F}}^2$$

The estimate of $\mathbf{P}$ is achieved by

$$\hat{\mathbf{P}} = (\tilde{\mathbf{Z}}_1 \tilde{\mathbf{Z}}_1^H)^{-1} \tilde{\mathbf{Z}}_1 \tilde{\mathbf{Z}}_2^H \tag{3.10}$$

In the noise-free case, $\tilde{\mathbf{B}}(\varphi) = \mathbf{P}_E \tilde{\boldsymbol{B}}_1(\varphi)$, and we partition $\mathbf{P}_E$ as

$$\mathbf{P}_E = \begin{bmatrix} \mathbf{P}_1 \\ \mathbf{P}_2 \\ \mathbf{P}_3 \\ \mathbf{P}_4 \end{bmatrix} \tag{3.11}$$

where $\mathbf{P}_i \in \mathbb{C}^{(N+1)\times K}\,(i=1,2,3,4)$. Then according to (3.4) and (3.7), we get

$$\mathbf{P}_1\tilde{\boldsymbol{B}}_1(\varphi)=\mathbf{B}_1 \tag{3.12.a}$$

$$\mathbf{P}_2\tilde{\boldsymbol{B}}_1(\varphi)=\mathbf{B}_1\boldsymbol{\alpha} \tag{3.12.b}$$

$$\mathbf{P}_3\tilde{\boldsymbol{B}}_1(\varphi)=\mathbf{B}_1\boldsymbol{\beta} \tag{3.12.c}$$

$$\mathbf{P}_4\tilde{\boldsymbol{B}}_1(\varphi)=\mathbf{B}_1\boldsymbol{\gamma} \tag{3.12.d}$$

Substitution of (3.12.a) into (3.12.d) yields

$$\mathbf{P}_1^{+}\mathbf{P}_4=\tilde{\boldsymbol{B}}_1(\varphi)\boldsymbol{\gamma}\tilde{\boldsymbol{B}}_1^{-1}(\varphi) \tag{3.13}$$

After the eigen-value decomposition of $\mathbf{P}_1^{+}\mathbf{P}_4$, the eigen-values correspond to the estimates of the diagonal elements of $\boldsymbol{\gamma}$, and the eigenvectors are the estimates of $\tilde{\boldsymbol{B}}_1(\varphi)$, which satisfies $\hat{\tilde{\boldsymbol{B}}}_1(\varphi)=\tilde{\boldsymbol{B}}_1(\varphi)\boldsymbol{\Pi}$, where $\boldsymbol{\Pi}$ is a permutation matrix, and $\boldsymbol{\Pi}^{-1}=\boldsymbol{\Pi}^{T}$. Then the estimate of $\boldsymbol{\gamma}$ satisfies $\hat{\boldsymbol{\gamma}}=\boldsymbol{\Pi}^{T}\boldsymbol{\gamma}\boldsymbol{\Pi}$.

To obtain automatically-paired 2D-DOA, we get $\hat{\tilde{\mathbf{B}}}(\varphi)=\hat{\mathbf{P}}_E\hat{\tilde{\boldsymbol{B}}}_1(\varphi)$ according to (3.7), and partition $\hat{\tilde{\mathbf{B}}}(\varphi)$ as

$$\hat{\tilde{\mathbf{B}}}(\varphi)=\begin{bmatrix}\hat{\mathbf{B}}_1\\ \hat{\mathbf{B}}_2\\ \hat{\mathbf{B}}_3\\ \hat{\mathbf{B}}_4\end{bmatrix} \tag{3.14}$$

In the noiseless case, $\mathbf{B}_2=\mathbf{B}_1\boldsymbol{\alpha}$, $\mathbf{B}_3=\mathbf{B}_1\boldsymbol{\beta}$, and $\mathbf{B}_4=\mathbf{B}_1\boldsymbol{\gamma}$, via $\mathbf{B}_1\boldsymbol{\alpha}/\mathbf{B}_1$ and $\mathbf{B}_1\boldsymbol{\beta}/\mathbf{B}_1$, $\boldsymbol{\alpha}$ and $\boldsymbol{\beta}$ can be obtained, where $/$ represents the division between diagonal elements of two matrices. The estimates of $\boldsymbol{\alpha}$ and $\boldsymbol{\beta}$ are $\hat{\boldsymbol{\alpha}}=\boldsymbol{\Pi}^{T}\boldsymbol{\alpha}\boldsymbol{\Pi}$ and $\hat{\boldsymbol{\beta}}=\boldsymbol{\Pi}^{T}\boldsymbol{\beta}\boldsymbol{\Pi}$, which can be achieved via $\hat{\mathbf{B}}_2/\hat{\mathbf{B}}_1$ and $\hat{\mathbf{B}}_3/\hat{\mathbf{B}}_1$, respectively.

Finally, according to the definition of $\mathbf{u}_k$, the elevation and azimuth angles are estimated by

$$\hat{\phi} = angle\ (\hat{\boldsymbol{\alpha}} + j\hat{\boldsymbol{\beta}}) \tag{3.15.a}$$

$$\hat{\varphi} = \sin^{-1}(\hat{\boldsymbol{\gamma}}) \tag{3.15.b}$$

Till now, we have derived the 2D-DOA estimation algorithm based on the Toeplitz Hermitian matrix representation for acoustic vector-sensor array. We summarize below,

Step 1: Construct the Toeplitz Hermitian matrix $\mathbf{Z}$ via (3.1) and (3.2);

Step 2: Partition $\mathbf{Z}$ to estimate $\hat{\mathbf{P}}_E$ via (3.8) and (3.10);

Step 3: Partition $\hat{\mathbf{P}}_E$ to get $\mathbf{P}_i \in \mathbb{C}^{(N+1)\times K}(i = 1,2,3,4)$, and obtain $\hat{\boldsymbol{\gamma}}$ and $\tilde{\boldsymbol{B}}_1(\varphi)$ via (3.11)-(3.13);

Step 4: Get $\hat{\mathbf{B}}_1$, $\hat{\mathbf{B}}_2$ and $\hat{\mathbf{B}}_3$ from (3.14) to obtain $\hat{\boldsymbol{\alpha}}$ and $\hat{\boldsymbol{\beta}}$, and finally estimate the elevation and azimuth angles using (3.15).

3.2.2.3 Complexity Analysis

The complexity of the proposed algorithm is $O\{36(N+1)^3 + 4K(N+1)^2 + 4K^2(N+1) + 3K^3\}$, while that of the spatial smoothing-based PM (SS-PM) and the spatial smoothing-based ESPRIT algorithm (SS-ESPRIT) are $O\{16(2N+1)^2 + 512N^3 + 64N^2K + 14NK^2 + 3K^3\}$ and $O\{16(2N+1)^2 + 1024N^3 + 6NK^2 + 2K^3\}$, respectively. It is apparent that the computational complexity of the proposed algorithm is significantly lower than that of SS-ESPRIT and SS-PM algorithms.

Figure 3.2 presents the complexity comparison among the proposed algorithm, SS-PM, and SS-ESPRIT algorithm, when *K*=3 for different values of *N*. Figure 3.3 depicts the complexity comparison when *N*=10 for different values of *K*.

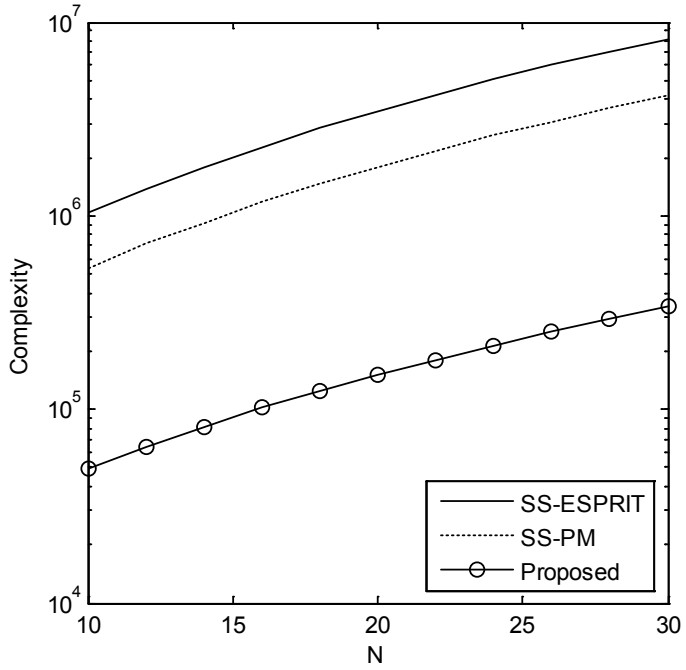

Figure 3.2 Complexity comparison for K=3 and different values of N

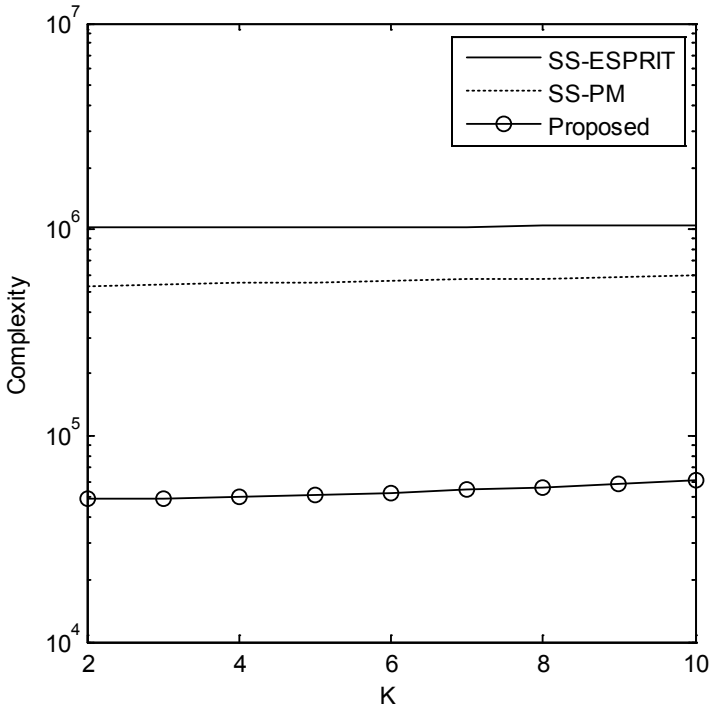

Figure 3.3 Complexity comparison for N=10 and different values of K

3.2.2.4 Advantages of the Proposed Algorithm

The proposed algorithm has the following advantages:

1) The computational complexity of the proposed algorithm is significantly lower than that of subspace-based methods

2) The proposed algorithm obtains the estimation results under a single snapshot

3) The proposed algorithm works well for coherent signals

4) The proposed algorithm can achieve automatically-paired 2D angle estimation

5) The proposed method has a better angle performance than spatial smoothing methods do.

3.2.3 Simulation Results

In this subsection, simulation results are presented to show the performance of the proposed DOA estimation technique as compared to some of the existing methods. In the experiment, we consider that there are two coherent signals sources with DOA (ϕ_1, φ_1)=(20°, 30°) and (ϕ_2, φ_2)=(50°, 60°). The root mean square error (RMSE) is used to evaluate the estimation performance in this thesis, which is defined as

$$RMSE = \frac{1}{K}\sum_{k=1}^{K}\sqrt{\frac{1}{L}\sum_{l=1}^{L}[(\hat{\phi}_{k,l}-\phi_k)^2+(\hat{\varphi}_{k,l}-\varphi_k)^2]}$$

where $\hat{\phi}_{k,l}$, $\hat{\varphi}_{k,l}$ are the estimates of ϕ_k, φ_k of the *l*th Monte Carlo trial.

Figures 3.4 and 3.5 depict angle estimation results of the proposed algorithm for two sources with SNR=15dB, and SNR=25dB. The array consists of *M*=17 sensors with one sensor at the origin and the number of snap-shots *L*=1. The elevation and azimuth angles can be clearly observed in these figures.

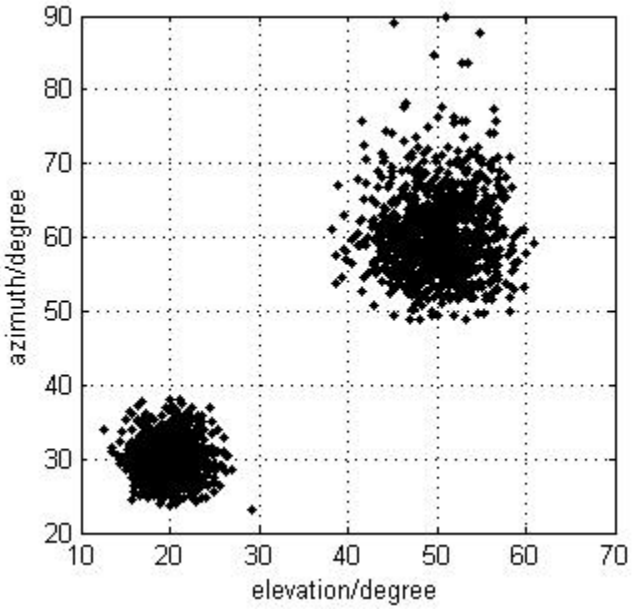

Figure 3.4 Estimation results of the proposed algorithm using acoustic vector sensor array containing 17 sensors with L=1 and SNR=15dB

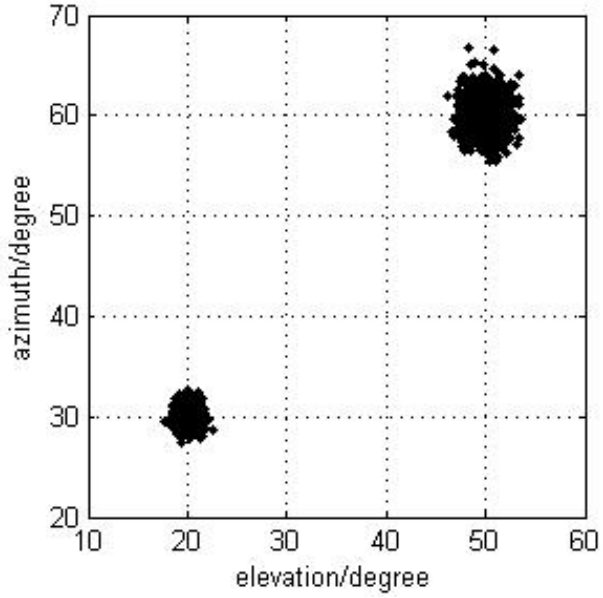

Figure 3.5 Estimation results of the proposed algorithm using acoustic vector sensor array containing 17 sensors with L=1 and SNR=25dB

Figure 3.6 presents the comparisons among the proposed algorithm, SS-PM, SS-ESPRIT [19], He's PM [29], PM of Palanisamy et al. [30] and CRB. The array consists of M=17 sensors with

one sensor at the origin and the number of snap-shots L=1. From Figure 3.6, we can observe that the angle estimation performance of the proposed algorithm is better than that of the other algorithms.

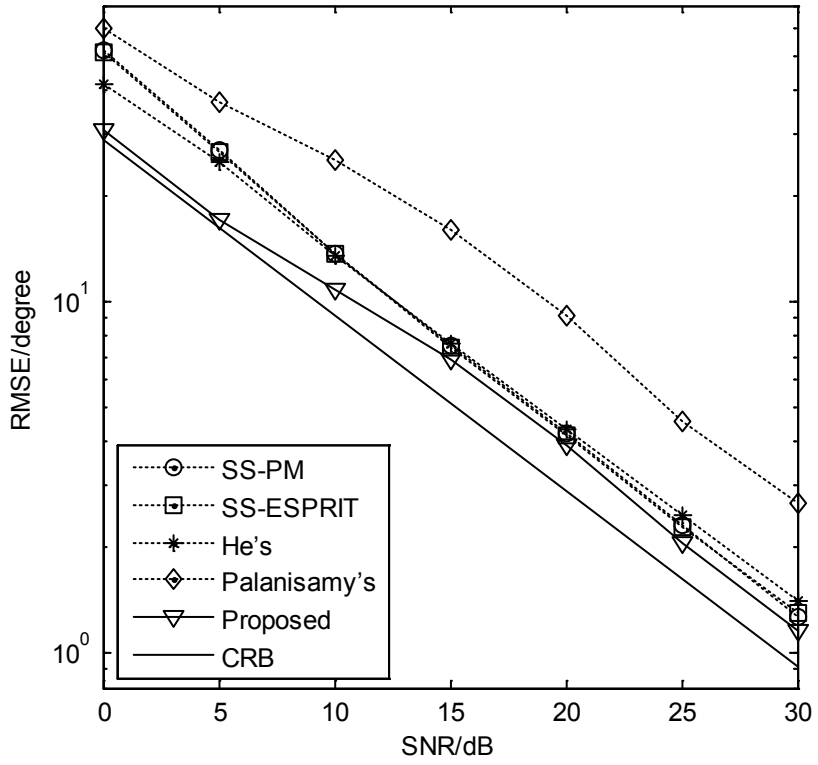

Figure 3.6 Estimation performance comparison between the proposed algorithm, SS-ESPRIT algorithm, SS-PM, He's PM, PM of Palanisamy et al. and CRB using acoustic vector sensor array containing 17 sensors with K=2 and L=1

Figure 3.7 shows the angle estimation performance of the proposed algorithm for different values of M and L=1. It is seen that the angle estimation performance of the proposed algorithm improves with increasing M.

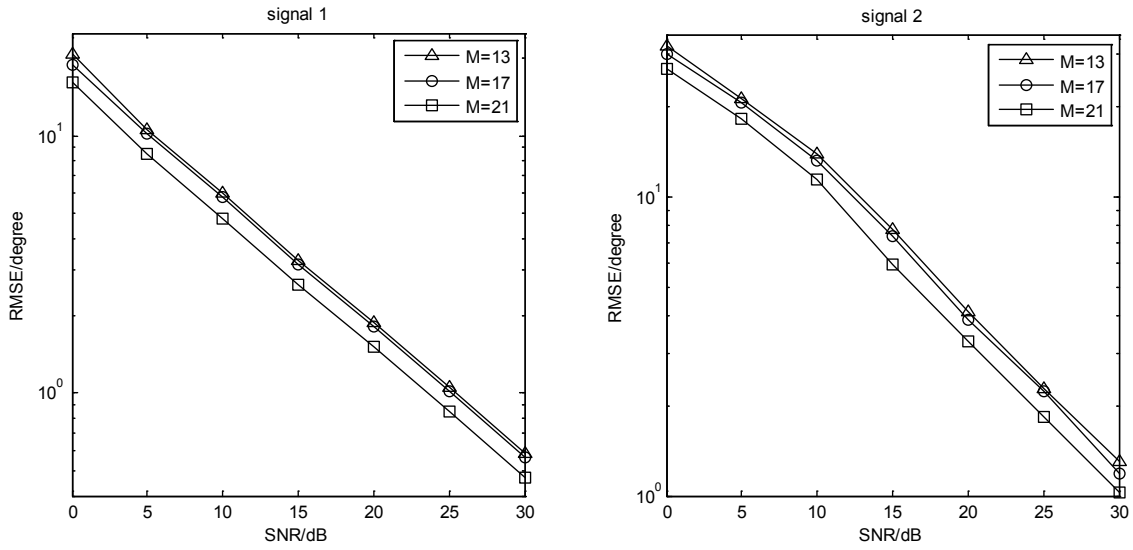

Figure 3.7 Estimation performance comparison of the proposed algorithm with L=1, K=2 and different values of M

In another experiment, we consider that there are three coherent signal sources with DOA (ϕ_1, φ_1)=(20°, 30°), (ϕ_2, φ_2)=(40°, 50°) and (ϕ_3, φ_3)=(60°, 70°), first and second signals being coherent and the third uncorrelated with the first and second signals.

Figure 3.8 shows the comparison among the proposed algorithm, SS-PM, SS-ESPRIT algorithm, and CRB. The array consists of M=31 sensors with one sensor at the origin and L=1. It is seen that the DOA estimation performance of the SS-PM and SS-ESPRIT algorithm hardly improves with increasing SNR, and their RMSEs at higher SNRs are approximately equal to their RMSEs at lower SNRs. Hence, the DOA estimation performance of the proposed algorithm is better than that of the other two algorithms.

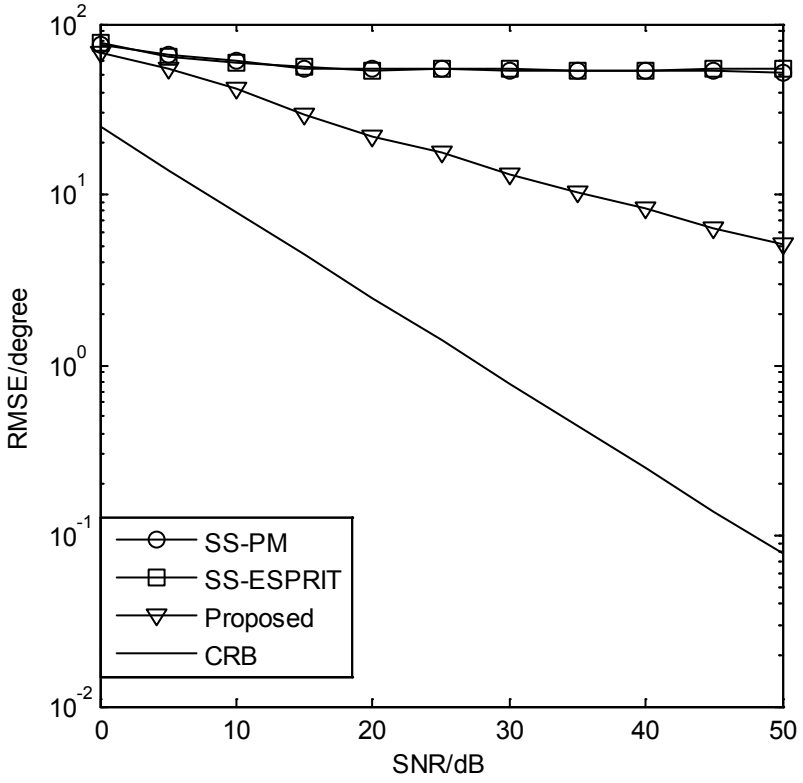

Figure 3.8 Estimation performance comparison between the proposed algorithm, SS-ESPRIT algorithm, SS-PM and CRB using acoustic vector sensor array containing 31 sensors with K=3 and L=1

In Figure 3.9, we consider that the array consists of M=31 sensors and the snap-shots L=50 in SS-PM and SS-ESPRIT algorithm while L=1 in our algorithm. It can be seen that when we increase the number of snap-shots in SS-PM and SS-ESPRIT algorithm, the performances of these two algorithms ameliorate, so the absence of enough snap-shots accounts for the degradation.

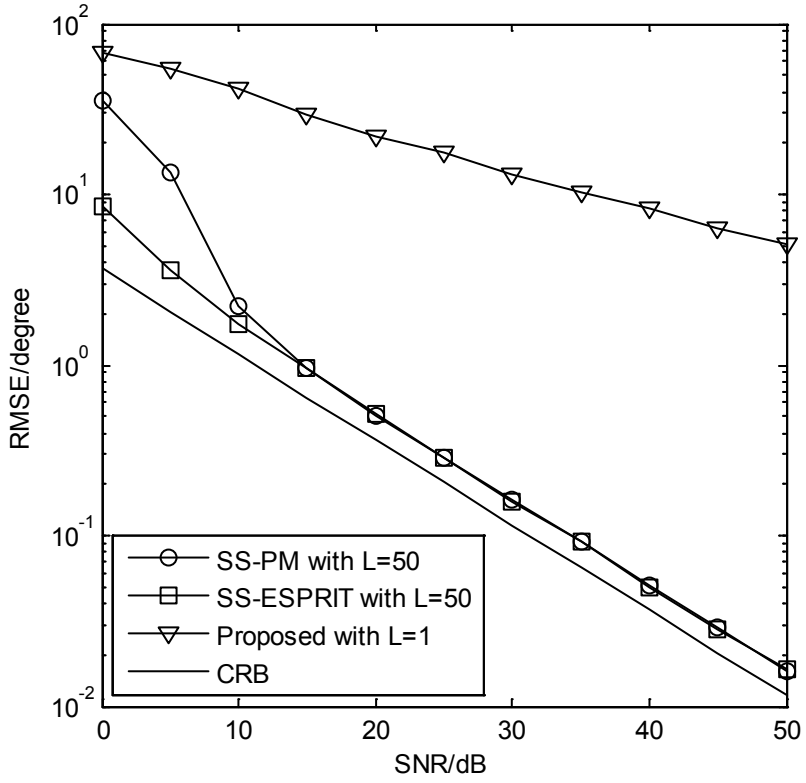

Figure 3.9 Estimation performance comparison between the proposed algorithm, SS-ESPRIT algorithm, SS-PM and CRB using acoustic vector sensor array containing 31 sensors with K=3 and L=50 in SS-PM and SS-ESPRIT algorithm while L=1 in the proposed algorithm

3.3 Improved 2D-DOA Estimation of Coherent Signals with Acoustic Vector-sensor Array Using Multiple Snapshots

In this section, we consider the problem of 2D-DOA estimation of coherent signals impinging on an L-shaped array of acoustic vector sensors, and propose an improved estimation algorithm based on the PM of Palanisamy et al. Compared with latter algorithm, the computational complexity of the proposed algorithm is lower and the angle estimation performance is better. Furthermore, the pair-matching problem that occurs in the PM of Palanisamy et al. is solved in our algorithm. The simulation results validate the effectiveness of the proposed algorithm.

3.3.1 Data Model

In order to compare the proposed algorithm with the PM of Palanisamy et al. [30], the same data model is considered, which differs from the data model introduced in Subsection 2.1. Consider that an L-shaped acoustic vector sensor array as shown in Figure 3.10 consists of 2(*M*-1) sensors, out of which (*M*-1) sensors of the array are located on the x-axis and *M* sensors located on the z-axis with an interelement spacing of *d* and a common reference sensor at the origin.

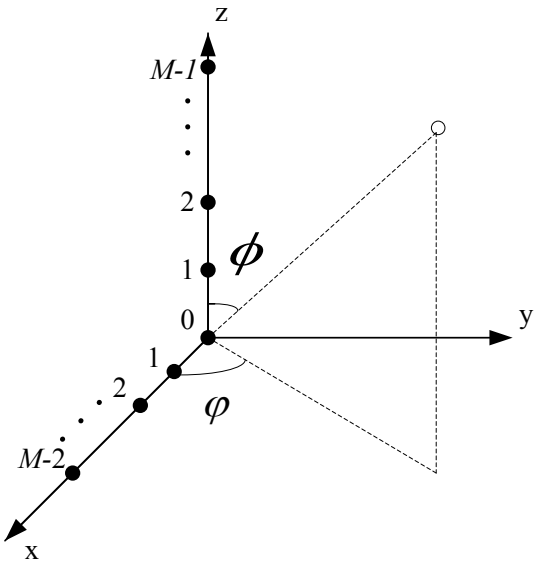

Figure 3.10 The structure of array

A total of *K* narrowband plane waves impinge on the L-shaped array, and we consider the signals in the far-field. Consider that the *k*th signal is arriving from direction (ϕ_k , φ_k), where φ_k and ϕ_k stand for the azimuth angle and the elevation angle, respectively. Each element of the acoustic vector array produces an output, which is a 4×1 vector, corresponding to the acoustic pressure and the acoustic particle velocity. The 4×1 array manifold corresponding to the *i*th signal is given by

$$\mathbf{c}(\phi_k, \varphi_k) = \begin{bmatrix} \sin\phi_k \cos\varphi_k \\ \sin\phi_k \sin\varphi_k \\ \cos\phi_k \\ 1 \end{bmatrix} = \begin{bmatrix} \alpha_k \\ \beta_k \\ \gamma_k \\ 1 \end{bmatrix} \quad \text{for } k=1, 2, \ldots, K \tag{3.16}$$

From [30], we know that the output at the *m*th sensor of the acoustic vector sensor array located on the x-axis can be expressed as

$$\begin{aligned} &\mathbf{x}_m(t) = \sum_{k=1}^{K} s_k(t) e^{jm\psi_k} \mathbf{c}(\phi_k, \varphi_k) + \mathbf{n}_{xm}(t) = \mathbf{B}_{x_m}^H \mathbf{s}(t) + \mathbf{n}_{xm}(t) \\ &for\ m = 0,1,...,M-2; \quad t = 1,2,...,L \end{aligned} \tag{3.17}$$

where $\psi_k = (2\pi d / \lambda)\alpha_k$, $\mathbf{B}_{x_i} = [e^{-ji\psi_1}\mathbf{c}(\phi_1,\varphi_1), e^{-ji\psi_2}\mathbf{c}(\phi_2,\varphi_2),...,e^{-ji\psi_K}\mathbf{c}(\phi_K,\varphi_K)]^T$ is a K×4 matrix, and $\mathbf{n}_{xm}(t)$ is a noise vector at the *m*th sensor of the acoustic vector sensor array along the x-axis. The entire output at all sensors located on the x-axis can be represented as

$$\mathbf{x}(t) = \mathbf{A}_x \mathbf{s}(t) + \mathbf{n}_x(t) \quad for\ t=1,2,\ldots,L \tag{3.18}$$

where $\mathbf{x}(t) = [\mathbf{x}_0^T(t), \mathbf{x}_1^T(t),..., \mathbf{x}_{M-2}^T(t)]^T$ is a 4(M-1)×1 vector,

$$\mathbf{A}_x = [\mathbf{q}_x(\phi_1,\varphi_1) \otimes \mathbf{c}(\phi_1,\varphi_1), \mathbf{q}_x(\phi_2,\varphi_2) \otimes \mathbf{c}(\phi_2,\varphi_2),..., \mathbf{q}_x(\phi_K,\varphi_K) \otimes \mathbf{c}(\phi_K,\varphi_K)]$$

is a 4(M-1)×K array manifold matrix of the acoustic vector sensor array along the x-axis and $\mathbf{q}_x(\phi_k,\varphi_k) = [1, e^{j\psi_k}, e^{j2\psi_k},..., e^{j(M-2)\psi_k}]^T$, $\mathbf{s}(t) = [s_1(t), s_2(t),..., s_K(t)]^T$ is the K×1 signal vector, and $\mathbf{n}_x(t) = [\mathbf{n}_{x0}^T(t), \mathbf{n}_{x1}^T(t),...\mathbf{n}_{x(M-2)}^T(t)]^T$ is the 4(M-1)×1 noise vector at the acoustic vector sensor array along the x-axis.

Similarly, the output at all sensors located on the z-axis can be represented as

$$\mathbf{z}(t) = \mathbf{A}_z \mathbf{s}(t) + \mathbf{n}_z(t) \quad \text{for } t=1,2,\ldots,L \tag{3.19}$$

where $\mathbf{z}(t) = [\mathbf{z}_0^T(t), \mathbf{z}_1^T(t),..., \mathbf{z}_{M-1}^T(t)]^T$ is a 4M×1 vector.

3.3.2 Improved DOA Estimation Algorithm

3.3.2.1 Decorrelation

We divide the source signals into p groups, and the signals in the same group are coherent, while being incoherent to the signals in the other groups. Let L_i be the number of coherent signals in the ith group and $L_{\max} = \max\{L_1, L_2, ..., L_p\}$.

***Remark A*:** The number of source signals D and the group number p can be pre-estimated via some available methods in [31-40].

Based on the noise assumption in Section 2.2, the cross-correlation $\mathbf{R}_{zx_k}$ between the observation vectors $\mathbf{z}(t)$ and $\mathbf{x}_i(t)$ can be expressed as

$$\mathbf{R}_{zx_i} = E[\mathbf{z}(t)\mathbf{x}_i^H(t)] = \mathbf{A}_z\mathbf{R}_s\mathbf{B}_{x_i} \quad \text{for } i=0,1,\ldots,M-2 \tag{3.20}$$

where $\mathbf{R}_s = E[\mathbf{s}(t)\mathbf{s}^H(t)]$ is a $K\times K$ autocorrelation matrix of the signal. The cross-correlation matrix $\mathbf{R}_{zx}$, which is a $4M\times 4(M-1)$ matrix, is formed by concatenating $\mathbf{R}_{zx_i}$ for $i=0,1,\ldots,M-2$, as

$$\mathbf{R}_{zx} = [\mathbf{R}_{zx_0}, \mathbf{R}_{zx_1}, ..., \mathbf{R}_{zx_{M-2}}] = \mathbf{A}_z\mathbf{R}_s\mathbf{A}_x^H \tag{3.21}$$

If all the source signals are incoherent, $rank\{\mathbf{R}_{zx}\} = D$ and the signal subspace can be formed without extra operations. However, if all or some of the source signals are coherent, then $rank\{\mathbf{R}_{zx}\} < D$ and the signal subspace cannot be formed directly. In order to decorrelate the coherent sources, we partition the cross-correlation matrix $\mathbf{R}_{zx}$ and form a new matrix $\mathbf{R}$ as follows

$$\mathbf{R} = [\mathbf{R}_{zx}^{(1)}, \mathbf{R}_{zx}^{(2)}, ..., \mathbf{R}_{zx}^{(L_{\max})}] \tag{3.22}$$

where the jth submatrix $\mathbf{R}_{zx}^{(j)}$ is formed from the $(4(j-1)+1)$th row to the $4(M-L_{\max}+j)$th row of $\mathbf{R}_{zx}$. The dimension of the matrix $\mathbf{R}$ is $4(M-L_{\max}+1)\times 4(M-1)L_{\max}$, and $\mathbf{R}$ can also be represented as

$$\mathbf{R} = \overline{\mathbf{A}}_z[\mathbf{\Phi}_z^0\mathbf{R}_s\mathbf{A}_x^H, \mathbf{\Phi}_z^1\mathbf{R}_s\mathbf{A}_x^H, ..., \mathbf{\Phi}_z^{L_{\max}-1}\mathbf{R}_s\mathbf{A}_x^H] = \overline{\mathbf{A}}_z\mathbf{\Psi}$$

where $\overline{\mathbf{A}}_z$ consists of the first $4(M- L_{\max}+1)$ rows of $\mathbf{A}_z$; $\mathbf{\Phi}_z = diag\{\exp(j2\pi d\cos\phi_1/\lambda), \exp(j2\pi d\cos\phi_2/\lambda), ..., \exp(j2\pi d\cos\phi_K/\lambda)\}$. Since *rank{* $\mathbf{\Phi}_z^i\mathbf{R}_s\mathbf{A}_x^H$ *}= min{rank(* $\mathbf{\Phi}_z^i$ *), rank(*$\mathbf{R}_s$*), rank(*$\mathbf{A}_x^H$*)}=min{D, rank(*$\mathbf{R}_s$*), D}= rank(*$\mathbf{R}_s$*)*, we get *rank{*$\mathbf{\Psi}$*}=p·rank(*$\mathbf{R}_s$*)*. Hence, we have *rank{*$\mathbf{R}$*}= min{rank{*$\overline{\mathbf{A}}_z$*},rank{*$\mathbf{\Psi}$*}}=min{K, p·rank(*$\mathbf{R}_s$*)}=D*, because *D*, *p*, *rank(*$\mathbf{R}_s$*)* always satisfy *p·rank(*$\mathbf{R}_s$*)* $\geq D$.

It is necessary to transform the matrix $\mathbf{R}$ using the exchange matrix $\mathbf{J}$ to bring the velocity components and the pressure components of the acoustic vector sensors together. We define a new transformed matrix $\tilde{\mathbf{R}}$ as

$$\tilde{\mathbf{R}} = \mathbf{J}^T\mathbf{R}$$

where $\mathbf{J} = [\mathbf{J}_1, \mathbf{J}_2, \mathbf{J}_3, \mathbf{J}_4]$, is a $4(M- L_{\max}+1)\times 4(M- L_{\max}+1)$ matrix, $\mathbf{J}_i = [e_i, e_{i+4}, e_{i+8}, ..., e_{i+4(M-L_{\max})}]$ for i=1,2,3,4, and e_i is the $4(M- L_{\max}+1)\times 1$ unit vector whose ith component is unity and all others are zero.

3.3.2.2 DOA Estimation

Next, we use the PM to estimate the 2D-DOAs. After the transformation applied to $\mathbf{R}$, the steering vector $\overline{\mathbf{A}}_z$ becomes

$$\tilde{\mathbf{A}}_z = \mathbf{J}^T\overline{\mathbf{A}}_z$$

where $\overline{\mathbf{A}}_z$ consists of the first $4(M- L_{\max}+1)$ rows of the array manifold matrix $\mathbf{A}_z$.

Partition the matrix $\tilde{\mathbf{A}}_z$ as

$$\tilde{\mathbf{A}}_z = \begin{bmatrix} \mathbf{A}_{z1} \\ \mathbf{A}_{z2} \\ \mathbf{A}_{z3} \\ \mathbf{A}_{z4} \end{bmatrix} = \begin{bmatrix} \mathbf{A}_{z4}\Gamma_1 \\ \mathbf{A}_{z4}\Gamma_2 \\ \mathbf{A}_{z4}\Gamma_3 \\ \mathbf{A}_{z4} \end{bmatrix} \tag{3.23}$$

where $\Gamma_1 = diag\{\alpha_1, \alpha_2, ..., \alpha_K\}$, $\Gamma_2 = diag\{\beta_1, \beta_2, ..., \beta_K\}$ and $\Gamma_3 = diag\{\gamma_1, \gamma_2, ..., \gamma_K\}$ are $K \times K$ diagonal matrices.

Because $\mathbf{A}_{z4}$ is a Vandermonde matrix with full rank K, $\mathbf{A}_{z4}$ can be partitioned as

$$\mathbf{A}_{z4} = \begin{bmatrix} \mathbf{A}_2 \\ \mathbf{A}_1 \end{bmatrix}$$

where $\mathbf{A}_1$ is a $K \times K$ nonsingular matrix, and $\mathbf{A}_2$ is a $[(M - L_{\max} + 1) - K] \times K$ matrix. $\tilde{\mathbf{A}}_z$ can also be expressed by

$$\tilde{\mathbf{A}}_z = \begin{bmatrix} \mathbf{A}_2\Gamma_1 \\ \mathbf{A}_1\Gamma_1 \\ \mathbf{A}_2\Gamma_2 \\ \mathbf{A}_1\Gamma_2 \\ \mathbf{A}_2\Gamma_3 \\ \mathbf{A}_1\Gamma_3 \\ \mathbf{A}_2 \\ \mathbf{A}_1 \end{bmatrix} = \begin{bmatrix} \mathbf{B}_2 \\ \mathbf{A}_1 \end{bmatrix}$$

where $\mathbf{B}_2 \in \mathbb{C}^{[4(M - L_{\max} + 1) - K] \times K}$ is a linear transformation of $\mathbf{A}_1$, namely,

$$\mathbf{B}_2 = \mathbf{P}^H \mathbf{A}_1$$

where $\mathbf{P} \in \mathbb{C}^{K \times [4(M - L_{\max} + 1) - K]}$ is the propagator matrix [18].

We define $\mathbf{P}_E = \begin{bmatrix} \mathbf{P}^H \\ \mathbf{I}_{K \times K} \end{bmatrix}$, then

$$\mathbf{P}_E \mathbf{A}_1 = \tilde{\mathbf{A}}_z \tag{3.24}$$

We partition $\mathbf{P}_E$ as

$$\mathbf{P}_E = \begin{bmatrix} \mathbf{P}_{E1} \\ \mathbf{P}_{E2} \\ \mathbf{P}_{E3} \\ \mathbf{P}_{E4} \end{bmatrix} \tag{3.25}$$

where $\mathbf{P}_{E1}, \mathbf{P}_{E2}, \mathbf{P}_{E3}, \mathbf{P}_{E4} \in \mathbb{C}^{(M-L_{\max}+1)\times K}$. Then according to (3.23) and (3.24), we get

$$\mathbf{P}_{E1} \mathbf{A}_1 = \mathbf{A}_{z4} \Gamma_1 \tag{3.26.a}$$

$$\mathbf{P}_{E2} \mathbf{A}_1 = \mathbf{A}_{z4} \Gamma_2 \tag{3.26.b}$$

$$\mathbf{P}_{E3} \mathbf{A}_1 = \mathbf{A}_{z4} \Gamma_3 \tag{3.26.c}$$

$$\mathbf{P}_{E4} \mathbf{A}_1 = \mathbf{A}_{z4} \tag{3.26.d}$$

Substituting (3.26.d) into (3.26.c), we obtain

$$\mathbf{P}_{E4}^{+} \mathbf{P}_{E3} = \mathbf{A}_1 \Gamma_3 \mathbf{A}_1^{-1} \tag{3.27}$$

After the eigen-value decomposition of $\mathbf{P}_{E4}^{+} \mathbf{P}_{E3}$, the eigen-values correspond to the diagonal elements of Γ_3, and the eigenvectors are the estimates of $\mathbf{A}_1$, which satisfies $\hat{\mathbf{A}}_1 = \mathbf{A}_1 \mathbf{\Pi}$, where $\mathbf{\Pi}$ is a permutation matrix, and $\mathbf{\Pi}^{-1} = \mathbf{\Pi}^T$.

***Remark B*:** Eq. (3.27) can also be represented as $\mathbf{P}_{E4}^{+} \mathbf{P}_{E3} \mathbf{A}_1 = \mathbf{A}_1 \Gamma_3$, where Γ_3 is a diagonal matrix consisting of the eigen-values of $\mathbf{P}_{E4}^{+} \mathbf{P}_{E3}$. Hence, it is obvious that the eigenvectors of $\mathbf{P}_{E4}^{+} \mathbf{P}_{E3}$ are the estimate of $\mathbf{A}_1$.

In order to obtain **P**, we partition the covariance matrix of the received data $\tilde{\mathbf{R}}$ as

$$\tilde{\mathbf{R}} = \begin{bmatrix} \mathbf{R}_2 \\ \mathbf{R}_1 \end{bmatrix} \tag{3.28}$$

where $\mathbf{R}_1 \in \mathbb{C}^{K\times[4(M-1)L_{\max}]}$, $\mathbf{R}_2 \in \mathbb{C}^{[4(M-L_{\max}+1)-K]\times[4(M-1)L_{\max}]}$ and

$$\mathbf{R}_2 = \mathbf{P}^H \mathbf{R}_1 \tag{3.29}$$

As described by (3.10), the estimate of $\mathbf{P}$ can be obtained via

$$\hat{\mathbf{P}} = \mathbf{R}_2 \mathbf{R}_1^H (\mathbf{R}_1 \mathbf{R}_1^H)^{-1} \tag{3.30}$$

According to (3.24), we get $\hat{\tilde{\mathbf{A}}}_z = \mathbf{P}_E \hat{\mathbf{A}}_1$, and partition $\hat{\tilde{\mathbf{A}}}_z$ as

$$\hat{\tilde{\mathbf{A}}}_z = \begin{bmatrix} \hat{\mathbf{A}}_{z1} \\ \hat{\mathbf{A}}_{z2} \\ \hat{\mathbf{A}}_{z3} \\ \hat{\mathbf{A}}_{z4} \end{bmatrix} \tag{3.31}$$

In the noise-free case, $\mathbf{A}_{z1} = \mathbf{A}_{z4}\Gamma_1$, $\mathbf{A}_{z2} = \mathbf{A}_{z4}\Gamma_2$, thereby

$$\Gamma_1 = \mathbf{A}_{z4}^{+}\mathbf{A}_{z1} \text{ and } \Gamma_2 = \mathbf{A}_{z4}^{+}\mathbf{A}_{z2} \tag{3.32}$$

Hence the estimates of Γ_1 and Γ_2 can be achieved by $\hat{\mathbf{A}}_{z4}^{+}\ \hat{\mathbf{A}}_{z1}$ and $\hat{\mathbf{A}}_{z4}^{+}\ \hat{\mathbf{A}}_{z2}$, respectively. Finally, according to the definition of $\mathbf{c}(\phi_k, \varphi_k)$ in (3.16), the elevation and azimuth angles are estimated by

$$\hat{\phi} = \cos^{-1}(\hat{\Gamma}_3) \tag{3.33.a}$$

$$\hat{\varphi} = angle\ (\hat{\Gamma}_1 + j\hat{\Gamma}_2) \tag{3.33.b}$$

Till now, we have obtained the improved PM-based 2D-DOA estimation of coherent signals using acoustic vector-sensor array. We give the major steps of the proposed algorithm below.

Step 1: Form the covariance matrix of the received data $\tilde{\mathbf{R}}$ using (3.20)-(3.22);

Step 2: Obtain the propagator matrix **P** using (3.28)-(3.30);

Step 3: Construct and partition $\mathbf{P}_E$ to get $\mathbf{P}_{E1}, \mathbf{P}_{E2}, \mathbf{P}_{E3}, \mathbf{P}_{E4}$, and obtain $\hat{\Gamma}_3$ and $\hat{\mathbf{A}}_1$ via (3.25)-(3.27);

Step 4: Get $\hat{\Gamma}_1$ and $\hat{\Gamma}_2$ from (3.31), and finally estimate the elevation and azimuth angles using (3.33)

3.3.2.3 Complexity Analysis

First, calculating $\tilde{\mathbf{R}}$ requires multiplications of order $O\{64(M-L_{\max}+1)^2(M-1)L_{\max} +16M(M-1)L\}$, and obtaining the propagator matrix **P** has computational complexity of $O\{16K(M-L_{\max}+1)(M-1)L_{\max}+4K^2(M-L_{\max}+1)\}$. Also, computing $\hat{\Gamma}_3$ and $\hat{\mathbf{A}}_1$ is of $O\{4K^2(M-L_{\max}+1)+2K^2\}$. Finally, estimating $\hat{\Gamma}_1$ and $\hat{\Gamma}_2$ requires $O\{10K^2(M-L_{\max}+1)+2K^2\}$ computations. Therefore, the computational load of the proposed algorithm is about $O\{64(M-L_{\max}+1)^2(M-1)L_{\max}+16M(M-1)L+4K^2+16K(M-L_{\max}+1)(M-1)L_{\max}+17K^2(M-L_{\max}+1)\}$, while the PM of Palanisamy et al. is $O\{64(M-L_{\max}+1)^2(M-1)L_{\max}+16M(M-1)L-3K^2+ 16K(M-L_{\max}+1)(M-1)L_{\max}+13K^2(M-L_{\max}+1)\}$ without considering the cost of extra computationally-expensive pair matching, where L denotes the number of snap-shots. The computational complexity of the proposed algorithm is lower.

3.3.2.4 Advantages of the Proposed Algorithm

The proposed algorithm has the following advantages.

1) The computational complexity of the proposed algorithm is smaller than that of the PM of Palanisamy et al.

2) The angle estimation performance of the proposed algorithm is better than that of the PM of Palanisamy et al.

3) The proposed algorithm achieves automatically-paired two-dimensional angle estimates.

4) The proposed algorithm can be used for the DOA estimation of coherent signals.

3.3.3 Simulation Results

In this subsection, simulation results are presented to show the performance of the proposed DOA estimation technique as compared to some of the existing methods. In the first experiment, we consider that there are two coherent signal sources with DOA (ϕ_1, φ_1)=(50°, 40°) and (ϕ_2, φ_2)=(60°, 50°). The array consists of 12 sensors with 7 sensors along the z-direction and 6 sensors along the x-direction and we define RMSE as

$$RMSE = \sqrt{1/2000 \sum_{n=1}^{2000} [(\hat{\phi}_{n,k} - \phi_k)^2 + (\hat{\varphi}_{n,k} - \varphi_k)^2]}$$

where $\hat{\phi}_{n,k}$, $\hat{\varphi}_{n,k}$ are the estimates of ϕ_k, φ_k of the *n*th Monte Carlo trial.

Figures 3.11 and 3.12 depict the angle estimation results of the proposed algorithm for two sources with *SNR*=0dB, snap-shots *L*=500, and *SNR*=15dB, *L*=500. The elevation and azimuth angles can be clearly observed.

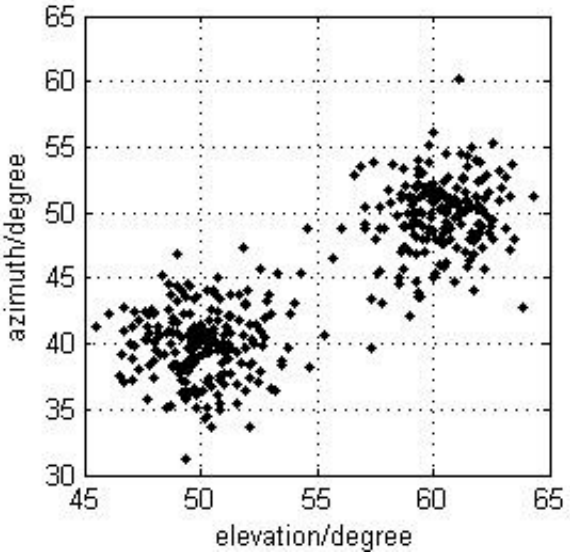

Figure 3.11 Estimation results of the proposed algorithm using acoustic vector sensor array containing 12 sensors with 7 sensors along z-direction and 6 sensors along x-direction with *L*=500, *K*=2 and SNR=0dB

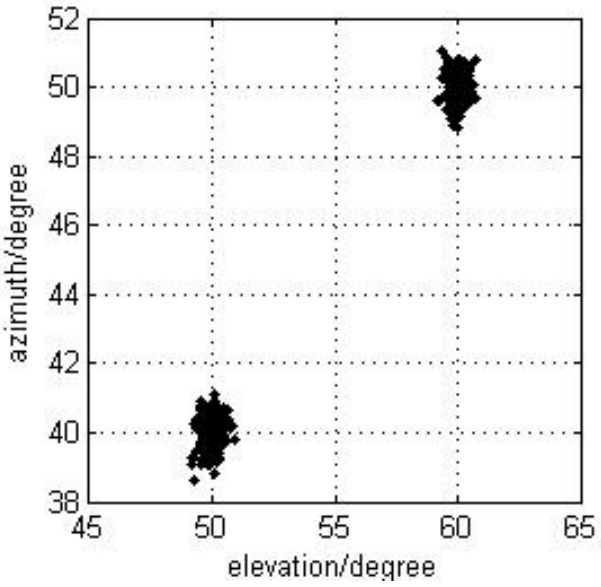

Figure 3.12 Estimation results of the proposed algorithm using acoustic vector sensor array containing 12 sensors with 7 sensors along z-direction and 6 sensors along x-direction with L=500, K=2 and SNR=15dB

Figure 3.13 presents the comparisons among the proposed algorithm, the PM of Palanisamy et al. and CRB. It is seen that the angle estimation performance of the proposed algorithm is better than that of the PM of Palanisamy et al.

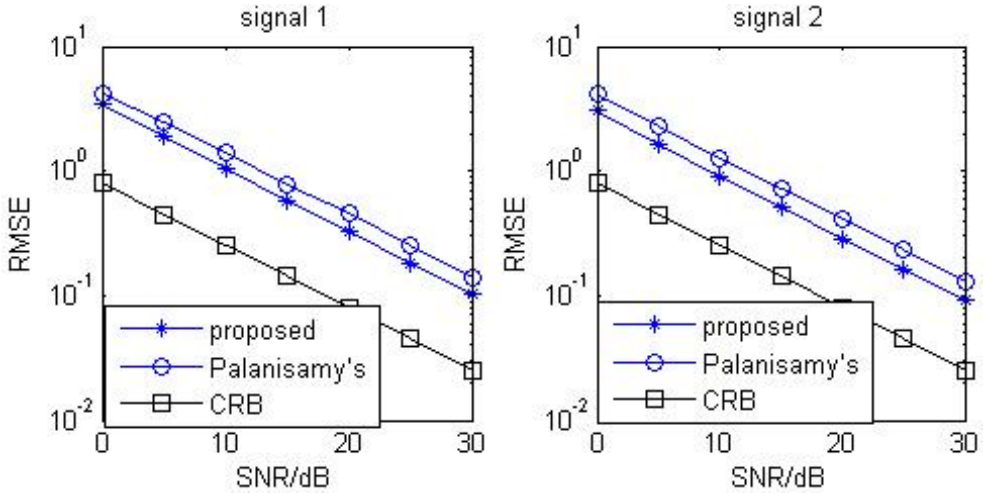

Figure 3.13 Estimation performance comparison between the proposed algorithm, the PM of Palanisamy et al. and CRB using acoustic vector sensor array containing 12 sensors with 7 sensors along z-direction and 6 sensors along x-direction with K=2 and L=500

Figure 3.14 presents the angle estimation performance of the proposed algorithm for different values of L. It is observed that the angle estimation performance of the proposed algorithm improves with increasing L.

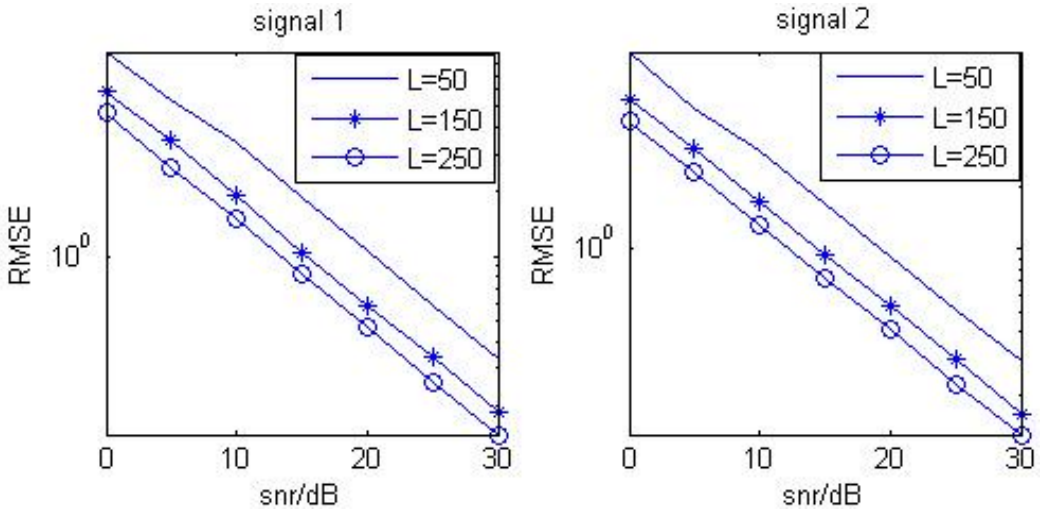

Figure 3.14 Estimation performance of the proposed algorithm with M=12, and K=2 for different values of L

In another experiment, we consider that there are K = 3 sources with DOA$(\phi_1, \varphi_1)=(50^\circ, 40^\circ)$, $(\phi_2, \varphi_2)=(60^\circ, 50^\circ)$ and $(\phi_3, \varphi_3)=(70^\circ, 60^\circ)$, second and third signals being coherent and the first being uncorrelated with the second and third signals. The array consists of 16 sensors of 9 sensors along z-direction and 8 sensors along x-direction.

Figures 3.15 and 3.16 depict the angle estimation results of the proposed algorithm for all three sources with SNR=0dB, L=500 and SNR=15dB, L=500. The estimated elevation and azimuth angles can be clearly observed.

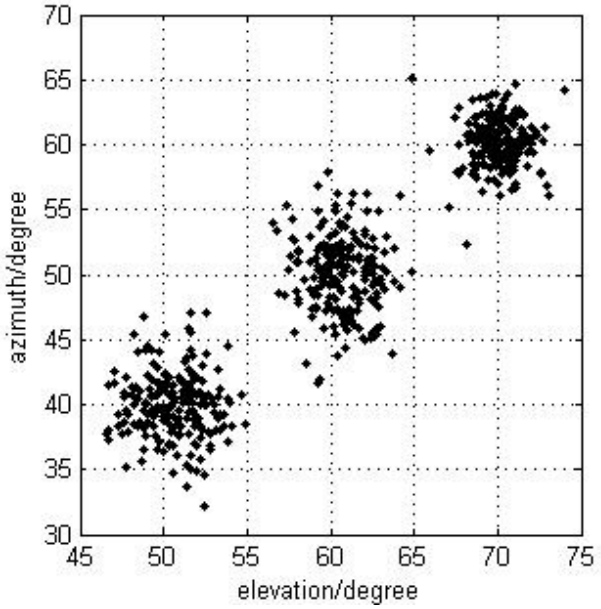

Figure 3.15 Estimation results of the proposed algorithm using acoustic vector sensor array containing 16 sensors of 9 sensors along z-direction and 8 sensors along x-direction with L=500, K=3 and SNR=0dB

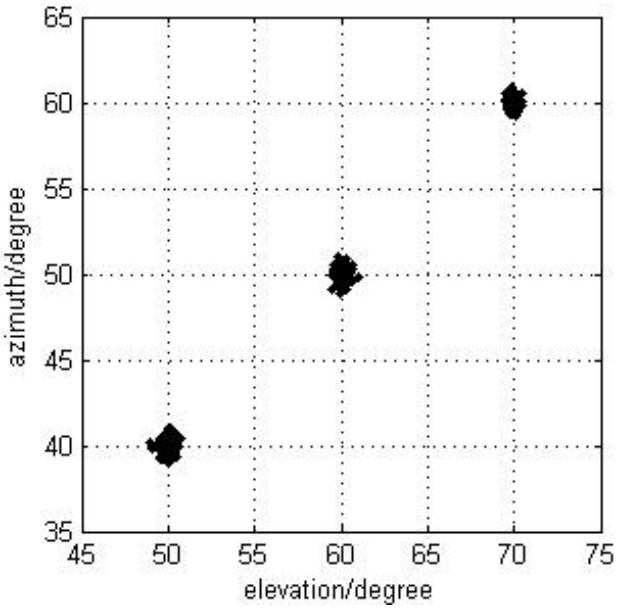

Figure 3.16 Estimation results of the proposed algorithm using acoustic vector sensor array containing 16 sensors of 9 sensors along z-direction and 8 sensors along x-direction with L=500, K=3 and SNR=15dB

Figure 3.17 shows the performance comparison of the proposed method with that of the SS-

PM [19], the He's PM [29], the PM of Palanisamy et al. [30] and the CRB. In the experiment of Figure 3.17, L=100 or L=200 snapshots. It is clearly seen that the estimation performance of the proposed algorithm is better than that of the SS-PM, the He's PM and the PM of Palanisamy et al., when the same snapshot number L=100 is used. Also, note that the estimation performance of the proposed algorithm with L=100 is very close to that of the PM of Palanisamy et al. with L=200. That's because the proposed algorithm is able to exploit all the useful received information to estimate $\hat{\Gamma}_1$, $\hat{\Gamma}_2$, and $\hat{\Gamma}_3$ by adding an identity matrix $\mathbf{I}_{K\times K}$ to expand the propagator matrix $\mathbf{P}$, so that $\mathbf{A}_{z1}, \mathbf{A}_{z2}, \mathbf{A}_{z3}$ and $\mathbf{A}_{z4}$ can be respectively considered as a whole in the following estimation step, rather than dividing each of them into two parts and just use one part to estimate $\hat{\Gamma}_1$, $\hat{\Gamma}_2$, and $\hat{\Gamma}_3$, which is actually used in the PM of Palanisamy et al. This expanding as well as the subsequent procedure can be regarded as doubling the useful information than the the PM of Palanisamy. It is also clear from Figure 3.17 that the estimation performance of the proposed algorithm improves with increasing the number of snapshots.

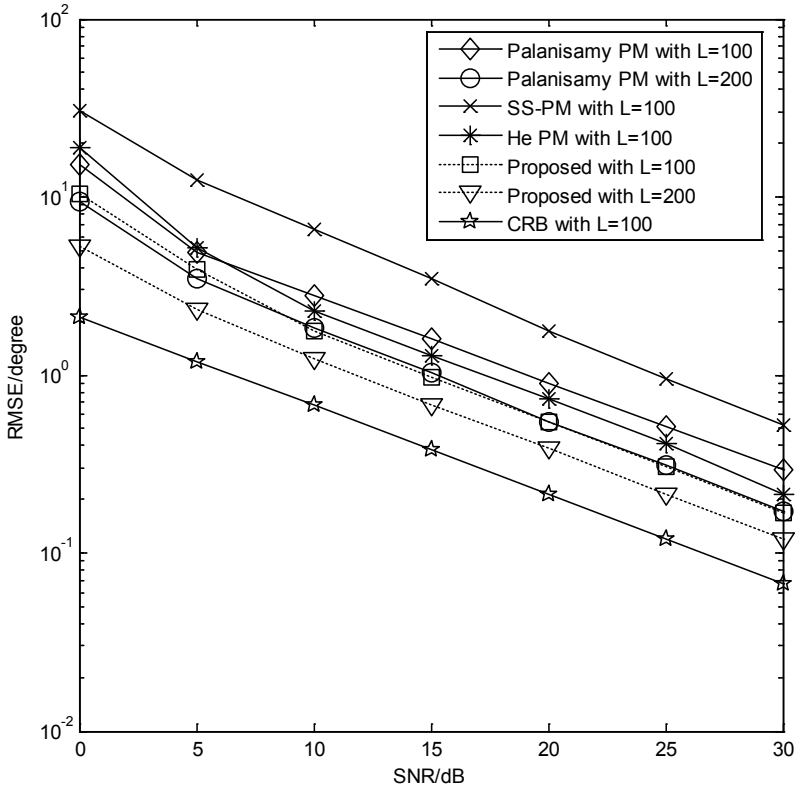

Figure 3.17 Estimation performance comparison between the proposed algorithm, SS-PM, He's PM, PM of Palanisamy et al. and CRB using acoustic vector sensor array containing 16 sensors of 9 sensors along z-direction and 8 sensors along x-direction with K=3 and L=100 or 200.

Figure 3.18 presents the angle estimation performance of the proposed algorithm for different values of L. It is observed that the angle estimation performance of the proposed algorithm improves with increasing L.

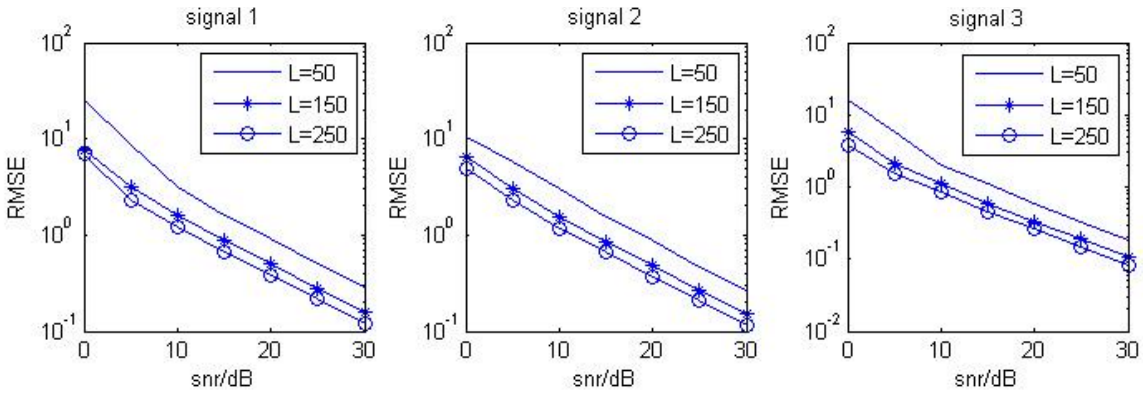

Figure 3.18 Estimation performance comparison of the proposed algorithm with M=15, K=3 and different values of L

3.4 Summary

In this chapter, we proposed two novel methods to enhance the 2D-DOA estimation performance for coherent incident sources using acoustic vector-sensor array.

In Section 3.2, a method which collects only a single snapshot to estimate the 2D-DOA of coherent incident sources is proposed by combining the PM with Toeplitz Hermitian matrix representation. This method has a better angle performance and less computational complexity than the traditional spatial smoothing methods.

Based on the PM of Palanisamy et al. [30], an improved 2D-DOA estimation algorithm of coherent signals impinging on an L-shaped acoustic vector-sensor array was presented in Section 3.3. Compared to the PM of Palanisamy et al., the proposed algorithm has the advantages of lower computational complexity, better estimation performance, and being able to acquire automatically-paired 2D-DOA estimates.

Chapter 4

4 2D-DOA Estimation of Noncircular Signals with Acoustic Vector-Sensor Array

4.1 Introduction

For a zero-mean Gaussian random vector $\mathbf{x}$, its covariance matrix is defined as $\mathbf{R} = E[\mathbf{x}\mathbf{x}^H]$ and complementary covariance matrix is defined as $\mathbf{C} = E[\mathbf{x}\mathbf{x}^T]$. In the past, it was often assumed that the complementary covariance vanishes, $\mathbf{C} = \mathbf{O}$, a case that is referred to as circular [46]. However, it has been shown that there are a number of situations in communications where this does not hold. For example, binary phase shift keying (BPSK) modulator, which is found to be bandwidth efficient in underwater communications [24], produces noncircular communication signals, in which case $\mathbf{C} \neq \mathbf{O}$. When dealing with the noncircular signals, a better 2D-DOA estimation performance can be achieved by taking the information contained in the complementary covariance into account.

In this chapter, the real-valued space PM and ESPRIT algorithm are proposed for 2D-DOA estimation of noncircular signals by using arbitrarily spaced acoustic vector sensor array. By exploiting the noncircularity of the incoming signals to increase the amount of effective data, the proposed algorithms can provide better 2D-DOA estimation performance with fewer snapshots, which means a relatively lower sample rate can be used in practical implementations. Compared with the traditional PM and ESPRIT, the proposed algorithms provide better estimation performance while at the same time having a similar computational complexity. Furthermore, the proposed algorithms are suitable for arbitrary arrays and yield paired azimuth and elevation angle estimates without requiring extra computationally-expensive pairing operations.

4.2 Data Model

Consider that a total of K plane acoustic waves impinge on an irregular array containing M acoustic vector sensors. We also consider the signals in the far-field, wherein the sources are far enough so that the arriving waves are essentially planes over the array. The noise is independent of the source, and is additive i.i.d. Gaussian with zeros mean and variance σ^2. Let the k-th signal

arrive from direction (ϕ_k, φ_k), where ϕ_k and φ_k stand for the azimuth and elevation angles, respectively. Let $\boldsymbol{\theta}_k = [\phi_k, \varphi_k]^{\mathrm{T}}$ denote the 2D-DOA of the *k*-th source. The output of the *m*-th acoustic vector sensor $\tilde{\mathbf{q}}_m(t)$ is shown to be

$$\tilde{\mathbf{q}}_m(t) = \begin{bmatrix} p_m(t) \\ x_m(t) \\ y_m(t) \\ z_m(t) \end{bmatrix} = \sum_{k=1}^{K} \begin{bmatrix} 1 \\ \cos\phi_k \cos\varphi_k \\ \sin\phi_k \cos\varphi_k \\ \sin\varphi_k \end{bmatrix} e^{-j2\pi\tau_{mk}} s_k(t) + \begin{bmatrix} n_{pm}(t) \\ n_{xm}(t) \\ n_{ym}(t) \\ n_{zm}(t) \end{bmatrix} \tag{4.1}$$

where $p(t)$ is the pressure measurement and $x(t)$, $y(t)$ and $z(t)$ represent the 3-D velocity measurements; $s_k(t)$ is the transmitted signal of the *k*-th source; τ_{mk} is the differential time delay of the *k*-th wave between the reference and the *m*-th sensor; $n_{pm}(t)$, $n_{xm}(t)$, $n_{ym}(t)$ and $n_{zm}(t)$ represent the noises. Then the output of the entire irregular array containing *M* acoustic vector sensors at time *t* is

$$\tilde{\mathbf{q}}(t) = \begin{bmatrix} \mathbf{p}(t) \\ \mathbf{x}(t) \\ \mathbf{y}(t) \\ \mathbf{z}(t) \end{bmatrix} = \begin{bmatrix} \tilde{\mathbf{A}}\mathbf{s}(t) \\ \tilde{\mathbf{A}}\boldsymbol{\Phi}_{\alpha}\mathbf{s}(t) \\ \tilde{\mathbf{A}}\boldsymbol{\Phi}_{\nu}\mathbf{s}(t) \\ \tilde{\mathbf{A}}\boldsymbol{\Phi}_{\omega}\mathbf{s}(t) \end{bmatrix} + \begin{bmatrix} \mathbf{n}_p(t) \\ \mathbf{n}_x(t) \\ \mathbf{n}_y(t) \\ \mathbf{n}_z(t) \end{bmatrix} \tag{4.2}$$

where $\mathbf{p}(t) = [p_1(t), ..., p_M(t)]^T$, $\mathbf{x}(t) = [x_1(t), ..., x_M(t)]^T$, $\mathbf{y}(t) = [y_1(t), ..., y_M(t)]^T$ and $\mathbf{z}(t) = [z_1(t), ..., z_M(t)]^T$; $\mathbf{s}(t) = [s_1(t), s_2(t), ..., s_K(t)]^T$; $\mathbf{n}_p(t) = [n_{p1}(t), n_{p2}(t), ..., n_{pM}(t)]^T$, $\mathbf{n}_x(t) = [n_{x1}(t), n_{x2}(t), ..., n_{xM}(t)]^T$, $\mathbf{n}_y(t) = [n_{y1}(t), n_{y2}(t), ..., n_{yM}(t)]^T$ and $\mathbf{n}_z(t) = [n_{z1}(t), n_{z2}(t), ..., n_{zM}(t)]^T$; $\boldsymbol{\Phi}_{\alpha} = diag\{\cos\phi_1 \cos\varphi_1, \cos\phi_2 \cos\varphi_2, ..., \cos\phi_K \cos\varphi_K\}$, $\boldsymbol{\Phi}_{\nu} = diag\{\sin\phi_1 \cos\varphi_1, \sin\phi_2 \cos\varphi_2, ..., \sin\phi_K \cos\varphi_K\}$ and $\boldsymbol{\Phi}_{\omega} = diag\{\sin\varphi_1, \sin\varphi_2, ..., \sin\varphi_K\}$. $\tilde{\mathbf{A}}$ is the steering matrix, which is given by $\tilde{\mathbf{A}} = [\mathbf{a}_1, \mathbf{a}_2, ..., \mathbf{a}_K]$ with $\mathbf{a}_k = [e^{-j2\pi\tau_{1k}}, e^{-j2\pi\tau_{2k}}, ...e^{-j2\pi\tau_{Mk}}]^T$.

By collecting *L* transmitted symbols, the output of the acoustic vector-sensor array is denoted as $\tilde{\mathbf{Q}} = [\tilde{\mathbf{q}}(1), \tilde{\mathbf{q}}(2), ..., \tilde{\mathbf{q}}(L)]$, which can be rewritten as

$$\tilde{\mathbf{Q}} = \begin{bmatrix} \mathbf{P} \\ \mathbf{X} \\ \mathbf{Y} \\ \mathbf{Z} \end{bmatrix} = \begin{bmatrix} \tilde{\mathbf{A}}\mathbf{S} \\ \tilde{\mathbf{A}}\boldsymbol{\Phi}_{\alpha}\mathbf{S} \\ \tilde{\mathbf{A}}\boldsymbol{\Phi}_{\nu}\mathbf{S} \\ \tilde{\mathbf{A}}\boldsymbol{\Phi}_{\omega}\mathbf{S} \end{bmatrix} + \mathbf{N} = \tilde{\mathbf{A}}_E\mathbf{S} + \tilde{\mathbf{N}} \tag{4.3}$$

where $\mathbf{P} = [\mathbf{p}(1), \mathbf{p}(2), ..., \mathbf{p}(L)]$, $\mathbf{X} = [\mathbf{x}(1), \mathbf{x}(2), ..., \mathbf{x}(L)]$, $\mathbf{Y} = [\mathbf{y}(1), \mathbf{y}(2), ..., \mathbf{y}(L)]$ and $\mathbf{Z} = [\mathbf{z}(1), \mathbf{z}(2), ..., \mathbf{z}(L)]$; $\mathbf{S} \in \mathbb{C}^{K \times L}$ is the source matrix for the L snapshots; $\tilde{\mathbf{N}} \in \mathbb{C}^{4M \times L}$ is the noise matrix.

A signal is said to be noncircular if its complementary covariance $\mathbf{C} \neq \mathbf{O}$ [25]. This statistical redundancy can be used to enhance the DOA estimation performance. According to the noncircular property, the source matrix can be denoted by

$$\mathbf{S} = \boldsymbol{\psi}\mathbf{S}_0 \tag{4.4}$$

where $\boldsymbol{\psi} = diag\{e^{i\psi_1}, ..., e^{i\psi_K}\}$ with $\psi_p \neq \psi_q$ for $p \neq q$ and $\mathbf{S}_0 \in \mathbb{R}^{K \times L}$ with $\mathbf{S}_0 = \mathbf{S}_0^{\ *}$.

In order to utilize the noncircularity of the signals, we first reconstruct and expand the output matrix $\tilde{\mathbf{Q}}$ to form $\mathbf{Q}$, which can be written as

$$\mathbf{Q} = \begin{bmatrix} \mathbf{P}_r \\ \mathbf{P}_j \\ \mathbf{X}_r \\ \mathbf{X}_j \\ \mathbf{Y}_r \\ \mathbf{Y}_j \\ \mathbf{Z}_r \\ \mathbf{Z}_j \end{bmatrix} = \begin{bmatrix} (\tilde{\mathbf{A}}\mathbf{S})_r \\ (\tilde{\mathbf{A}}\mathbf{S})_j \\ (\tilde{\mathbf{A}}\boldsymbol{\Phi}_{\alpha}\mathbf{S})_r \\ (\tilde{\mathbf{A}}\boldsymbol{\Phi}_{\alpha}\mathbf{S})_j \\ (\tilde{\mathbf{A}}\boldsymbol{\Phi}_{\nu}\mathbf{S})_r \\ (\tilde{\mathbf{A}}\boldsymbol{\Phi}_{\nu}\mathbf{S})_j \\ (\tilde{\mathbf{A}}\boldsymbol{\Phi}_{\omega}\mathbf{S})_r \\ (\tilde{\mathbf{A}}\boldsymbol{\Phi}_{\omega}\mathbf{S})_j \end{bmatrix} + \mathbf{N} \tag{4.5}$$

where subscripts r and j are the real and imaginary parts of the complex matrix, respectively. Substituting (4.4) into (4.5), $\mathbf{Q}$ can be simplified as

$$\mathbf{Q}=\begin{bmatrix}\begin{bmatrix}(\tilde{\mathbf{A}}\boldsymbol{\psi})_r\\(\tilde{\mathbf{A}}\boldsymbol{\psi})_j\end{bmatrix}\mathbf{S}_0\\\begin{bmatrix}(\tilde{\mathbf{A}}\boldsymbol{\psi})_r\\(\tilde{\mathbf{A}}\boldsymbol{\psi})_j\end{bmatrix}\boldsymbol{\Phi}_\alpha\mathbf{S}_0\\\begin{bmatrix}(\tilde{\mathbf{A}}\boldsymbol{\psi})_r\\(\tilde{\mathbf{A}}\boldsymbol{\psi})_j\end{bmatrix}\boldsymbol{\Phi}_\nu\mathbf{S}_0\\\begin{bmatrix}(\tilde{\mathbf{A}}\boldsymbol{\psi})_r\\(\tilde{\mathbf{A}}\boldsymbol{\psi})_j\end{bmatrix}\boldsymbol{\Phi}_\omega\mathbf{S}_0\end{bmatrix}+\mathbf{N}=\begin{bmatrix}\mathbf{A}\mathbf{S}_0\\\mathbf{A}\boldsymbol{\Phi}_\alpha\mathbf{S}_0\\\mathbf{A}\boldsymbol{\Phi}_\nu\mathbf{S}_0\\\mathbf{A}\boldsymbol{\Phi}_\omega\mathbf{S}_0\end{bmatrix}+\mathbf{N}=\mathbf{A}_E\mathbf{S}_0+\mathbf{N} \tag{4.6}$$

where $\mathbf{A}=\begin{bmatrix}(\tilde{\mathbf{A}}\boldsymbol{\psi})_r^T & (\tilde{\mathbf{A}}\boldsymbol{\psi})_j^T\end{bmatrix}^T$. This process of reconstruction increases the effective data for the next step of the 2D-DOA estimation. In other words, it is equivalent to enlarging the array aperture, which is actually twice as much as the original data if the noncircularity had not been utilized. This increase of effective data makes it possible to achieve a better 2D-DOA estimation performance, which means we can use relatively lower sampling rate in practical implementations.

4.3 2D-NC-PM based on Acoustic Vector-Sensor Array

4.3.1 DOA Estimation Using 2D-NC-PM

In the section, we use PM to estimate the 2D-DOAs. Partition the matrix $\mathbf{A}_E$ as

$$\mathbf{A}_E=\begin{bmatrix}\mathbf{A}_1\\\mathbf{A}_2\end{bmatrix} \tag{4.7}$$

where $\mathbf{A}_1$ is a $K\times K$ nonsingular matrix, $\mathbf{A}_2$ is a $(8M-K)\times K$ matrix. Then $\mathbf{A}_2$ is a linear transformation of $\mathbf{A}_1$,

$$\mathbf{A}_2=\mathbf{P}^H\mathbf{A}_1 \tag{4.8}$$

where $\mathbf{P}\in\mathbb{C}^{K\times(8M-K)}$ is the propagator matrix. We define $\mathbf{P}_E=\begin{bmatrix}\mathbf{I}_{K\times K}\\\mathbf{P}^H\end{bmatrix}$; then,

$$\mathbf{A}_E = \mathbf{P}_E \mathbf{A}_1 \tag{4.9}$$

We denote the covariance matrix of the received data by $\mathbf{R}_E$, which we partition as

$$\mathbf{R}_E = \begin{bmatrix} \mathbf{R}_1 & \mathbf{R}_2 \end{bmatrix} \tag{4.10}$$

where $\mathbf{R}_1 \in \mathbb{C}^{8M \times K}$ and $\mathbf{R}_2 \in \mathbb{C}^{8M \times (8M-K)}$. In the noise-free case, we can obtain

$$\mathbf{R}_2 = \mathbf{R}_1 \mathbf{P} \tag{4.11}$$

Actually, there is always noise, and the propagator matrix can be estimated by the following minimization problem

$$J_{csm}(\mathbf{P}) = \left\| \mathbf{R}_2 - \mathbf{R}_1 \mathbf{P} \right\|_{\mathrm{F}}^2$$

The estimate of $\mathbf{P}$ is then given by

$$\hat{\mathbf{P}} = (\mathbf{R}_1^{\mathrm{H}} \mathbf{R}_1)^{-1} \mathbf{R}_1^{\mathrm{H}} \mathbf{R}_2 \tag{4.12}$$

In the practical implementation, the covariance matrix $\mathbf{R}_E$ can be estimated through $\hat{\mathbf{R}}_E = \mathbf{Q}\mathbf{Q}^H / L$. Next, we use the estimated propagator $\hat{\mathbf{P}}$ to obtain 2D-DOA estimates. In the noise-free case, $\mathbf{P}_E$ can be partitioned as

$$\mathbf{P}_E = \begin{bmatrix} \mathbf{P}_1 \\ \mathbf{P}_2 \\ \mathbf{P}_3 \\ \mathbf{P}_4 \end{bmatrix} \qquad \mathbf{P}_1, \mathbf{P}_2, \mathbf{P}_3, \mathbf{P}_4 \in \mathbb{C}^{2M \times K} \tag{4.13}$$

Using (4.9) and (4.13), we obtian

$$\mathbf{A} = \mathbf{P}_1 \mathbf{A}_1 \tag{4.14.a}$$

$$\mathbf{A}\boldsymbol{\Phi}_{\omega} = \mathbf{P}_4 \mathbf{A}_1 \tag{4.14.b}$$

Then, it's easy to derive the relation from (4.14)

$$\mathbf{P}_1^{+}\mathbf{P}_4 = \mathbf{A}_1\mathbf{\Phi}_\omega\mathbf{A}_1^{-1} \tag{4.15}$$

After the eigen-value decomposition of $\mathbf{P}_1^{+}\mathbf{P}_4$, the eigen-values correspond to the diagonal elements of $\mathbf{\Phi}_\omega$, and the eigenvectors are the estimate of $\mathbf{A}_1$, namely, $\hat{\mathbf{A}}_1 = \mathbf{A}_1\mathbf{\Pi}$, where $\mathbf{\Pi}$ is a permutation matrix, and $\mathbf{\Pi}^{-1} = \mathbf{\Pi}^T$; then the estimate of $\mathbf{\Phi}_\omega$ is $\hat{\mathbf{\Phi}}_\omega = \mathbf{\Pi}\mathbf{\Phi}_\omega\mathbf{\Pi}$.

Now we consider estimating $\mathbf{\Phi}_\alpha$ and $\mathbf{\Phi}_\nu$. Substituting the estimated propagator $\hat{\mathbf{P}}$ and $\hat{\mathbf{A}}_1$ into (4.9), we can get the estimate of $\mathbf{A}_E$, namely, $\hat{\mathbf{A}}_E$ by

$$\hat{\mathbf{A}}_E = \hat{\mathbf{P}}_E\hat{\mathbf{A}}_1 \tag{4.16}$$

and then partition the estimated $\hat{\mathbf{A}}_E$ as

$$\hat{\mathbf{A}}_E = \begin{bmatrix} \hat{\mathbf{A}} \\ \hat{\mathbf{A}}\hat{\mathbf{\Phi}}_\alpha \\ \hat{\mathbf{A}}\hat{\mathbf{\Phi}}_\nu \\ \hat{\mathbf{A}}\hat{\mathbf{\Phi}}_\omega \end{bmatrix} \tag{4.17}$$

Define

$$\mathbf{B}_1 \triangleq \hat{\mathbf{A}},\ \mathbf{B}_2 \triangleq \hat{\mathbf{A}}\hat{\mathbf{\Phi}}_\alpha \text{ and } \mathbf{B}_3 \triangleq \hat{\mathbf{A}}\hat{\mathbf{\Phi}}_\nu \tag{4.18}$$

$\hat{\mathbf{\Phi}}_\alpha$ and $\hat{\mathbf{\Phi}}_\nu$ can be obtained via $\mathbf{B}_1^{+}\mathbf{B}_2$ and $\mathbf{B}_1^{+}\mathbf{B}_3$.

Finally, by exploiting the definition of $\mathbf{\Phi}_\alpha$, $\mathbf{\Phi}_\nu$ and $\mathbf{\Phi}_\omega$ in (4.2), the elevation and azimuth angles are estimated by

$$\hat{\phi} = angle(\hat{\mathbf{\Phi}}_\alpha + j\hat{\mathbf{\Phi}}_\nu) \tag{4.19.a}$$

$$\hat{\varphi} = \sin^{-1}(\hat{\mathbf{\Phi}}_\omega) \tag{4.19.b}$$

Since the column ambiguity doesn't exist in acquiring $\hat{\mathbf{\Phi}}_\alpha$, $\hat{\mathbf{\Phi}}_\nu$ and $\hat{\mathbf{\Phi}}_\omega$, the proposed algorithm gives automatically-paired azimuth and elevation angles without requiring extra computationally expensive pairing operations.

Till now, we have achieved the 2D-NC-PM algorithm for acoustic vector-sensor array. We give the major steps of the proposed algorithm below.

Step 1: Construct the data matrix $\mathbf{Q}$ via (4.5) and estimate the covariance matrix $\mathbf{R}_E$ through $\hat{\mathbf{R}}_E = \mathbf{Q}\mathbf{Q}^H / L$.

Step 2: Partition $\hat{\mathbf{R}}_E$ to estimate $\mathbf{P}_E$ via (4.10) and (4.12).

Step 3: Partition $\hat{\mathbf{P}}_E$ to get $\mathbf{P}_1, \mathbf{P}_2, \mathbf{P}_3, \mathbf{P}_4$ via (4.13), obtain $\hat{\mathbf{\Phi}}_\omega$ and $\hat{\mathbf{A}}_1$ by performing the eigenvalue decomposition to $\mathbf{P}_1^+ \mathbf{P}_4$.

Step 4: Get the estimate of $\mathbf{A}_E$ from (4.16), and partition it to obtain $\hat{\mathbf{\Phi}}_\alpha$ and $\hat{\mathbf{\Phi}}_\nu$ from (4.18), and finally estimate elevation and azimuth angles via (4.19).

4.3.2 Advantages of 2D-NC-PM Algorithm

The proposed algorithm has the following advantages:

1) The angle estimation performance of the proposed algorithm is better than that of the traditional PM, which will be seen in the simulation section (Section 4.3.3).
2) The proposed algorithm is suitable for arbitrary array geometry.
3) The proposed algorithm can achieve automatically paired two-dimensional angle estimates.

4.3.3 Simulation Results

In this subsection, simulation results are presented to show the performance of the proposed DOA estimation technique as compared to some of the existing methods. We consider that there are K = 3 sources with DOA (ϕ_1, φ_1)= $(10^\circ, -10^\circ)$, (ϕ_2, φ_2)=$(30^\circ, 30^\circ)$ and (ϕ_3, φ_3)= $(40^\circ, 50^\circ)$. Define RMSE as

$$RMSE = \frac{1}{K} \sum_{k=1}^{K} \sqrt{\frac{1}{N} \sum_{n=1}^{N} [(\hat{\phi}_{k,n} - \phi_k)^2 + (\hat{\varphi}_{k,n} - \varphi_k)^2]}$$

where $\hat{\phi}_{k,n}, \hat{\varphi}_{k,n}$ are the estimates of ϕ_k, φ_k of the n-th Monte Carlo trial.

Figure 4.1 depicts the angle estimation results from the proposed algorithm for all the three sources with M=10, L=200, SNR= 0dB and M=10, L=100, SNR= 20dB. It is seen that the elevation and azimuth angles can be clearly observed.

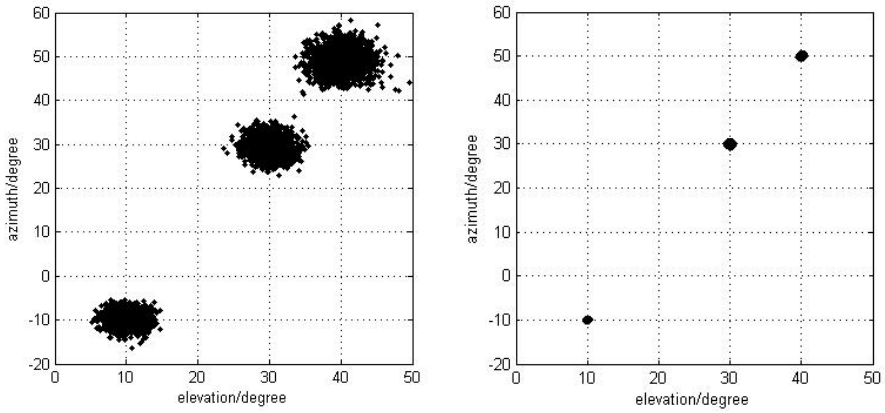

Figure 4.1 Estimation results of the proposed algorithm using 10 sensors with L=200, SNR= 0dB and L=100, SNR= 20dB

Figures 4.2 and 4.3 present comparisons of the estimation performance among the proposed algorithm, traditional PM and CRB. From these figures, we can observe that the angle estimation performance from the proposed algorithm is better than that of traditional PM.

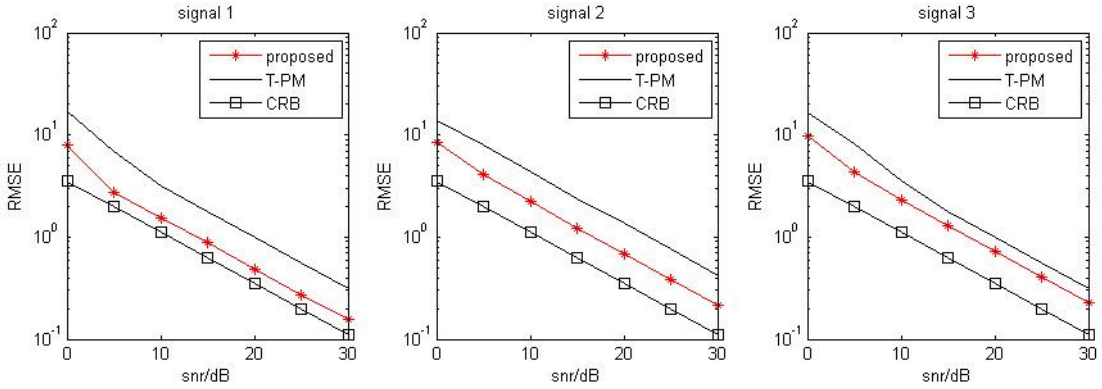

Figure 4.2 Estimation performance comparison between the proposed algorithm, traditional PM and CRB using 6 sensors with K=3 and L=50

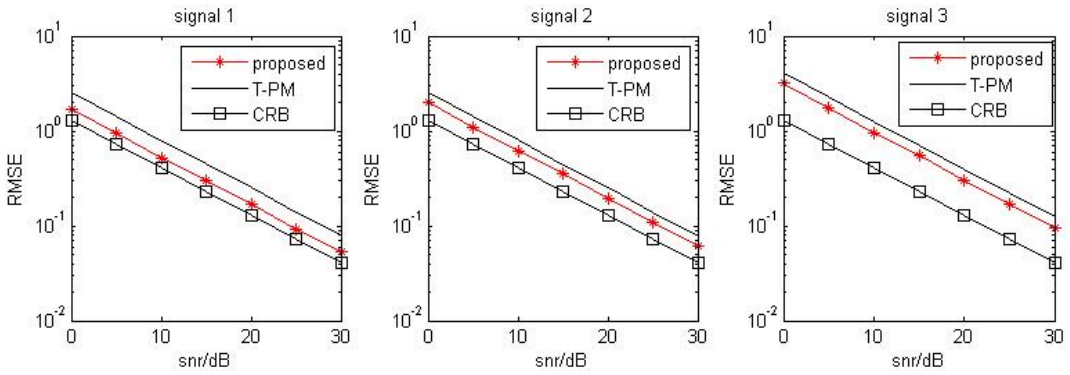

Figure 4.3 Estimation performance comparison between the proposed algorithm, traditional PM and CRB using 10 sensors with K=3 and L=200

Figure 4.4 presents the angle estimation performance of the proposed algorithm with M = 10, K = 3 and different values of L. It is seen from the figure that the angle estimation performance of the proposed algorithm improves with increasing L.

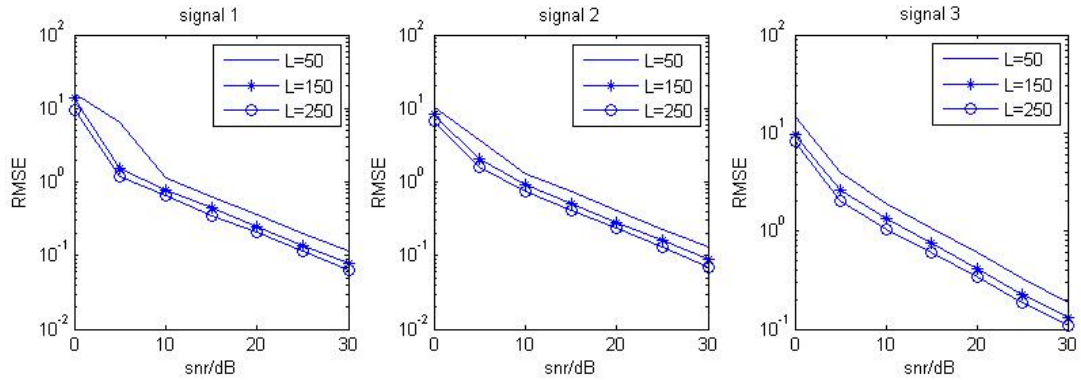

Figure 4.4 Estimation performance comparison of the proposed algorithm with M=10, K=3 and different values of L

Figure 4.5 shows the angle estimation performance of the proposed algorithm with L = 100, K = 3 for different M. It is observed that the angle estimation performance of the proposed algorithm improves with increasing the number of sensors.

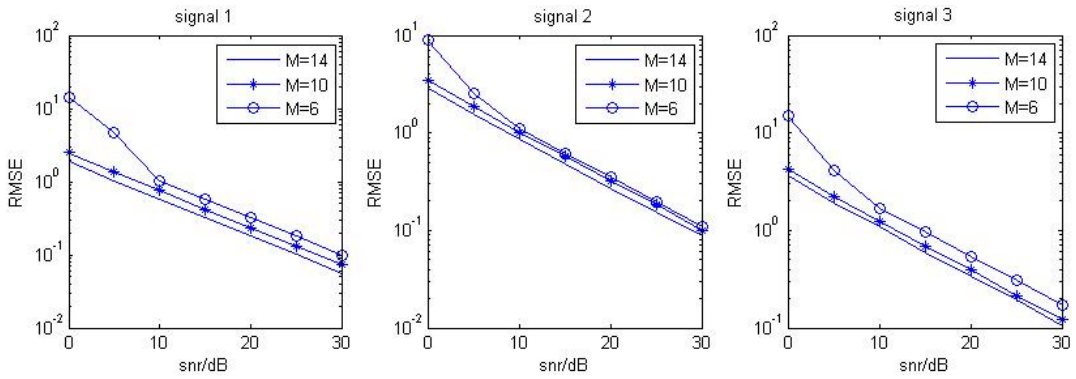

Figure 4.5 Estimation performance comparison of the proposed algorithm with L=100, K=3 and different values of M

4.4 2D-NC-ESPRIT based on Acoustic Vector-Sensor Array

4.4.1 DOA Estimation Using 2D-NC- ESPRIT

Here we use the ESPRIT method to estimate the 2D-DOAs. By performing the eigenvalue decomposition of $\mathbf{R}_E$, we obtain

$$\mathbf{R}_E = \mathbf{E}_s \mathbf{D}_s \mathbf{E}_s^H + \mathbf{E}_n \mathbf{D}_n \mathbf{E}_n^H \tag{4.20}$$

where $\mathbf{D}_s$ denotes a $K \times K$ diagonal matrix formed by the K largest eigenvalues, $\mathbf{D}_n$ denotes a diagonal matrix formed by (8M-K) smaller eigenvalues, $\mathbf{E}_s$ contains the eigenvectors corresponding to the K largest eigenvalues, and $\mathbf{E}_n$ represents the remaining eigenvectors. Note that $\mathbf{E}_s$ and $\mathbf{E}_n$ represent the signal and noise subspaces, respectively. It is well known that there exists a nonsingular $K \times K$ linear transform matrix $\mathbf{T}$ such that

$$\mathbf{E}_s = \mathbf{A}_E \mathbf{T} \tag{4.21}$$

We partition $\mathbf{E}_s$ as

$$\mathbf{E}_s = \begin{bmatrix} \mathbf{E}_1 & \mathbf{E}_2 & \mathbf{E}_3 & \mathbf{E}_4 \end{bmatrix}^T$$

where $\mathbf{E}_1 = \mathbf{AT}$, $\mathbf{E}_2 = \mathbf{A}\boldsymbol{\Phi}_\alpha\mathbf{T}$, $\mathbf{E}_3 = \mathbf{A}\boldsymbol{\Phi}_\nu\mathbf{T}$ and $\mathbf{E}_4 = \mathbf{A}\boldsymbol{\Phi}_\omega\mathbf{T}$. It is easy to verify that the eigenvalues of $\mathbf{E}_1^+\mathbf{E}_4$ correspond to the diagonal elements of $\boldsymbol{\Phi}_\omega$, and the eigenvectors are the estimate of $\mathbf{T}$, namely, $\hat{\mathbf{T}} = \mathbf{T}\boldsymbol{\Pi}$, where $\boldsymbol{\Pi}$ is a permutation matrix, and $\boldsymbol{\Pi}^{-1} = \boldsymbol{\Pi}^T$. Then the estimate of $\boldsymbol{\Phi}_\omega$ is given by $\hat{\boldsymbol{\Phi}}_\omega = \boldsymbol{\Pi}\boldsymbol{\Phi}_\omega\boldsymbol{\Pi}$. Thus, the elevation angles can be estimated by

$$\hat{\varphi}_k = \sin^{-1}(\hat{\omega}(\boldsymbol{\theta}_k)) \tag{4.22}$$

where $\hat{\omega}(\boldsymbol{\theta}_k)$ is the *k*-th diagonal element of $\hat{\boldsymbol{\Phi}}_\omega$.

The azimuth angles could be obtained by exploiting the inherent relations of the estimate $\hat{\mathbf{A}}_E$ of $\mathbf{A}_E$. Note that $\hat{\mathbf{A}}_E$ can be obtained from (4.17), that is, $\hat{\mathbf{A}}_E = \mathbf{E}_s\hat{\mathbf{T}}^{-1}$. Obviously, $\hat{\boldsymbol{\Phi}}_\alpha$, the estimate of $\boldsymbol{\Phi}_\alpha$, can be estimated by $\hat{\mathbf{A}}_E^+(1:2M,:)\hat{\mathbf{A}}_E(2M+1:4M,:)$, and $\hat{\boldsymbol{\Phi}}_\nu$, the estimates of $\boldsymbol{\Phi}_\nu$, can then be obtained via $\hat{\mathbf{A}}_E^+(1:2M,:)\hat{\mathbf{A}}_E(4M+1:6M,:)$. Finally, the azimuth angles are estimated as

$$\hat{\phi}_k = angle(\hat{\alpha}(\boldsymbol{\theta}_k) + j\hat{\nu}(\boldsymbol{\theta}_k)) \tag{4.23}$$

where $\hat{\alpha}(\boldsymbol{\theta}_k)$ and $\hat{\nu}(\boldsymbol{\theta}_k)$ are the *k*-th diagonal element of $\hat{\boldsymbol{\Phi}}_\alpha$ and that of $\hat{\boldsymbol{\Phi}}_\nu$, respectively. The covariance matrix $\mathbf{R}_E$ of the received signal can be estimated by $\hat{\mathbf{R}}_E = \mathbf{QQ}^H / L$.

In summary, the implementation of our algorithm contains the following four major steps:

Step 1: Construct the data matrix $\mathbf{Q}$ via (4.5) and estimate the covariance matrix $\mathbf{R}_E$ through $\hat{\mathbf{R}}_E = \mathbf{QQ}^H / L$.

Step 2: Perform eigenvalue decomposition to the covariance matrix $\hat{\mathbf{R}}_E$ to get the estimate $\mathbf{E}_s$ via (4.20).

Step 3: Partition $\mathbf{E}_s$ to obtain the estimates of $\boldsymbol{\Phi}_\omega$ and $\mathbf{T}$, and then estimate the elevation angles via (4.22).

Step 4: Obtain $\hat{\mathbf{A}}_E$ from (4.21), and estimate the azimuth angles via (4.23).

4.4.2 Complexity Analysis

Let us now consider the computational complexity of the proposed algorithm. First, calculating $\mathbf{R}_E$ requires multiplications of order $O(64M^2L)$, and decomposing $\mathbf{R}_E$ has computational complexity of $O(512M^3)$. Also, computing $\hat{\mathbf{\Phi}}_\omega$ is of $O(6MK^2+2K^3)$. Finally, estimating $\hat{\mathbf{\Phi}}_\alpha$ and $\hat{\mathbf{\Phi}}_\nu$ requires $O(20MK^2+2K^3)$ computations. Therefore, the computational load of the proposed algorithm is about $O(64M^2L+512M^3+26MK^2+4K^3)$. Considering that each complexity of the complex multiplication is four times that of a real-valued multiplication, one can show that the traditional complex ESPRIT algorithm needs $O(64M^2L+256M^3+52MK^2+32K^3)$ real multiplications. Figure 4.6 presents the complexity comparison between the proposed algorithm and the traditional complex ESPRIT algorithm for K=3, L=100 and different values of M. From Figure 4.6, we see that the computational complexity of the proposed algorithm is only slightly larger than that of the traditional ESPRIT algorithm.

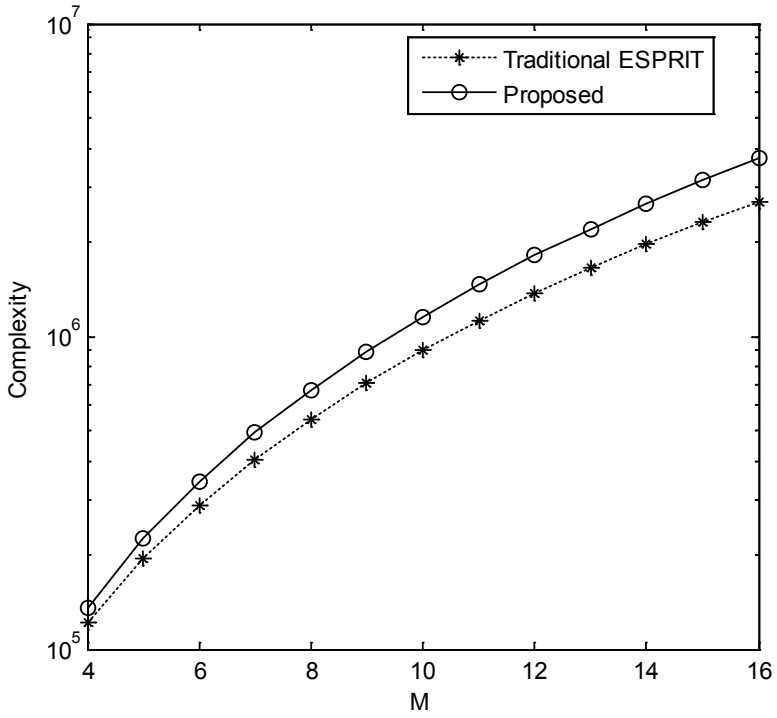

Figure 4.6 Complexity comparison for K=3, L=100 and different values of M

4.4.3 Advantages of 2D-NC- ESPRIT Algorithm

The proposed algorithm in this section has the following advantages.

1) The angle estimation performance of the proposed algorithm is better than that of traditional ESPRIT algorithm, which will be shown in the simulation section (Section 4.4.4).

2) The proposed algorithm is suitable for arbitrary arrays without knowing the locations of sensors.

3) The proposed algorithm can obtain automatically-paired two-dimensional angle estimates.

4.4.4 Simulation Results

In this subsection, simulation results are presented to show the performance of the proposed DOA estimation technique as compared to some of the existing methods. We consider that there are K = 3 sources with DOA $(\phi_1, \varphi_1) = (10^\circ, -10^\circ)$, $(\phi_2, \varphi_2) = (30^\circ, 30^\circ)$ and $(\phi_3, \varphi_3) = (40^\circ, 50^\circ)$ and define RMSE as

$$RMSE = \frac{1}{K}\sum_{k=1}^{K}\sqrt{\frac{1}{N}\sum_{n=1}^{N}[(\hat{\phi}_{k,n} - \phi_k)^2 + (\hat{\varphi}_{k,n} - \varphi_k)^2]}$$

where $\hat{\phi}_{k,n}, \hat{\varphi}_{k,n}$ are the estimation of ϕ_k, φ_k of the nth Monte Carlo trial.

Figure 4.7 depicts the angle estimation results of the proposed algorithm for the all three sources with M=10, L=200, SNR= 20dB. It is seen that the elevation and azimuth angles can be clearly observed.

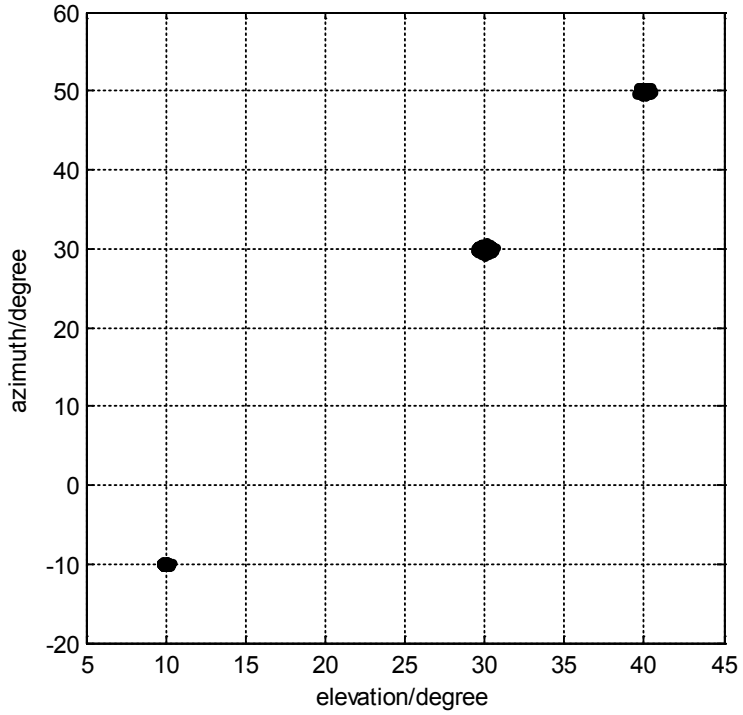

Figure 4.7 Estimation results of the proposed algorithm using 10 sensors with L=200 and SNR= 20dB.

Figure 4.8 presents a comparison of the estimation performance of the proposed method with that of the traditional ESPRIT algorithm using acoustic vector sensor array, as well as CRB. In our experiment of Figure 4.8, an acoustic vector sensor array of 10 sensors is employed, along with L=100 or 200 snapshots. It is clearly seen that the estimation performance of the proposed algorithm is better than that of the traditional ESPRIT algorithm when the same number of snapshots are adopted. Note that the estimation performance of the proposed algorithm with L=100 is close to that of the traditional ESPRIT algorithm with L=200, indicating that the effective data used for 2D-DOA estimation has been increased by utilizing the noncircularity of the source signals in the proposed algorithm. It is also clear from in Figure 4.8 that the estimation performance of the proposed algorithm improves with increasing number of snapshots.

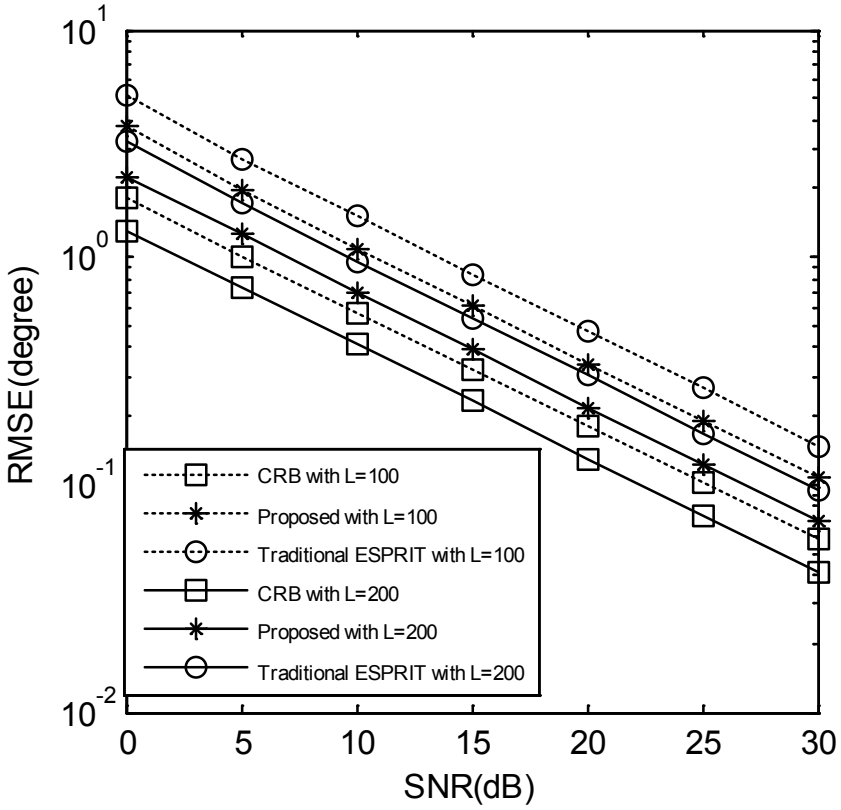

Figure 4.8 Estimation performance comparison between the proposed algorithm, traditional ESPRIT algorithm and CRB using 10 sensors with L=100 or 200.

Figure 4.9 presents the angle estimation performance of the proposed algorithm with M = 10, K = 3 and different values of L. It is observed that the angle estimation performance of the proposed algorithm improves with increasing the number of snapshots.

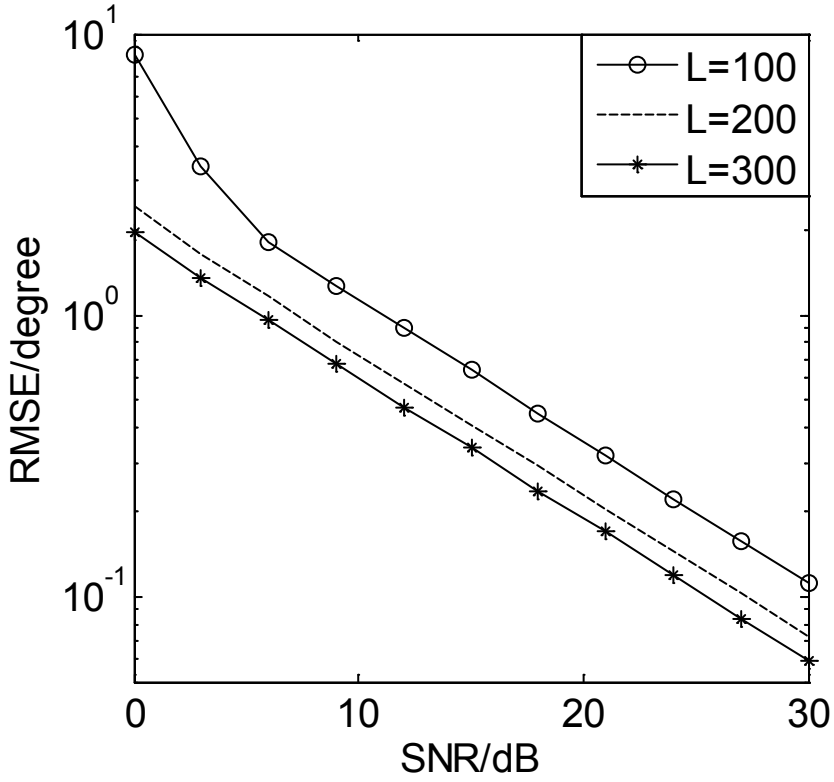

Figure 4.9 Estimation performance comparison of the proposed algorithm with M=10 and different values of L.

Figure 4.10 shows the angle estimation performance of the proposed algorithm with L = 100, K = 3 and different values of M. It is seen that the angle estimation performance of the proposed algorithm improves with increasing number of sensors.

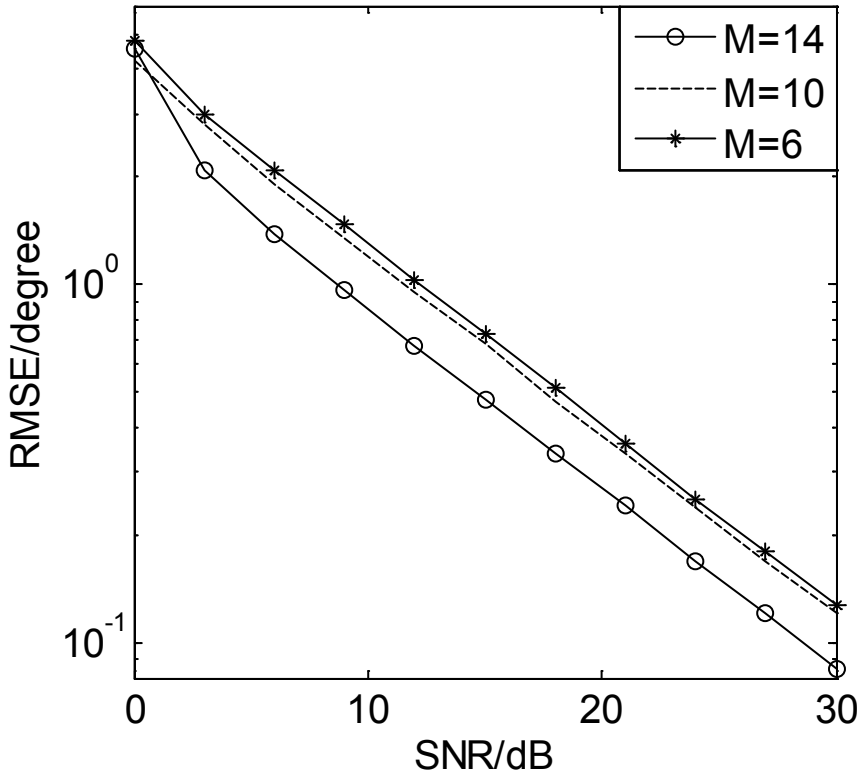

Figure 4.10 Estimation performance comparison of the proposed algorithm with L=100 and different values of M.

4.5 Summary

In this chapter, we have proposed real-valued space PM and ESPRIT algorithms for 2D-DOA estimation using arbitrarily spaced acoustic vector-sensor array. By exploiting the noncircularity of the incoming signals to increase the amount of effective data, the proposed algorithms provide better 2D-DOA estimation performance with fewer snapshots, which means a relatively lower sample rate can be used in practical implementations. Compared with the traditional PM and ESPRIT, the proposed algorithms provide better estimation performance while having similar computational complexity. Furthermore, the proposed algorithms are suitable for arbitrary arrays and yield paired azimuth and elevation estimation angles without requiring the extra computationally-expensive pairing operations.

Chapter 5

5 Conclusion and Future Work

5.1 Conclusion

This thesis has been concerned with the 2D-DOA estimation problem using acoustic vector-sensor array for coherent signals and noncircular signals.

For the coherent signals, two 2D-DOA estimation algorithms have been proposed. In the first algorithm, only a single snapshot is employed to estimate the 2D-DOA, while the second, an improved 2D-DOA estimation algorithm of coherent signals based on the PM of Palanisamy et al. has been proposed. Compared to the PM of Palanisamy et al., the proposed algorithm has a lower computational complexity as well as better estimation performance, and is able to acquire automatically-paired 2D-DOA estimation.

As for noncircular signals, we have proposed real-valued space PM and ESPRIT algorithms for 2D-DOA estimation using arbitrarily spaced acoustic vector-sensor array. By exploiting the noncircularity of the incoming signals to increase the amount of effective data, the proposed algorithms provide better 2D-DOA estimation performance with fewer snapshots, which means a relatively lower sample rate can be used in practical implementations. Compared with the traditional PM and ESPRIT, the proposed algorithms provide a better estimation performance while having similar computational complexity. Furthermore, the proposed algorithms are suitable for arbitrary arrays and yield paired azimuth and elevation angle estimates without requiring the extra computationally-expensive pairing operations.

5.2 Future Work

During my two years of study, some efficient algorithms have been proposed to deal with 2D-DOA estimation problem of coherent and noncircular incident sources using acoustic vector-sensor array. There are still some issues that require further investigation.

The two algorithms for coherent signals presented in this thesis use uniform linear array and L-shaped array to estimate the 2D-DOAs. However, due to the complexity of the underwater

environment, these two special arrays may be difficult to be realized in practical situations. Therefore, it is necessary to develop new methods using different types of arrays, especially arbitrarily spaced array.

Regarding noncircular signals, we have proposed the PM and ESPRIT-based real-valued space algorithms to estimate 2D-DOAs. Actually, there exist many super-resolution DOA estimation techniques such as MUSIC. By exploiting the noncircularity of the incoming signals in these super-resolution DOA estimation techniques, we can achieve more accurate estimation performance.

The noise is assumed to be additive *i.i.d.* Gaussian within this thesis, which, however, is almost impossible in practical submarine environment. Hence, it's meaningful to extend the proposed methods to different types of noise models.

References

[1] Nehorai, Arye; Paldi, E., "Acoustic vector-sensor array processing," *IEEE Transactions on Signal Processing,* vol.42, no.9, pp.2481-2491, Sep 1994.

[2] B. Hochwald and A. Nehorai, “Identifiability in array processing models with vector-sensor applications,” *IEEE Trans. Signal Process.*, vol. 44, no. 1, pp. 83–95, Jan. 1996.

[3] Nehorai, Arye; Paldi, E., "Acoustic vector sensor array processing," in Proc. of *1992 Conference Record of The Twenty-Sixth Asilomar Conference on Signals, Systems and Computers*, vol.1, pp.192-198, Oct 1992.

[4] G. Sun, D. Yang, and L. Zhang, “Maximum likelihood ratio detection and maximum likelihood DOA estimation based on the vector hydrophone,” *Acta Acustical*, 2003, 28(1):66–72.

[5] Hawkes, M.; Nehorai, Arye, "Acoustic vector-sensor beamforming and Capon direction estimation," *IEEE Trans. Signal Processing*, vol.46, no.9, pp.2291-2304, Sep 1998.

[6] Wong, K.T.; Zoltowski, M.D., "Self-initiating MUSIC-based direction finding in underwater acoustic particle velocity-field beamspace," *IEEE Journal of Oceanic Engineering*, vol.25, no.2, pp.262-273, April 2000.

[7] Wong, K.T.; Zoltowski, M.D., "Root-MUSIC-based azimuth-elevation angle-of-arrival estimation with uniformly spaced but arbitrarily oriented velocity hydrophones," *IEEE Transactions on Signal Processing*, vol.47, no.12, pp.3250-3260, Dec 1999.

[8] He, J.; Jiang, S.; Wang, J.; Liu, Z., "Direction finding in spatially correlated noise fields with arbitrarily-spaced and far-separated subarrays at unknown locations," *IET* in *Radar, Sonar & Navigation*, vol.3, no.3, pp.278-284, June 2009.

[9] Wong, K.T.; Zoltowski, M.D., "Closed-form underwater acoustic direction-finding with arbitrarily spaced vector hydrophones at unknown locations," *IEEE Journal of Oceanic Engineering*, vol.22, no.3, pp.566-575, Jul 1997.

[10] Wong, K.T.; Zoltowski, M.D., "Extended-aperture underwater acoustic multisource azimuth/elevation direction-finding using uniformly but sparsely spaced vector hydrophones," *IEEE Journal of Oceanic Engineering*, vol.22, no.4, pp.659-672, Oct 1997.

[11] Han Chen; Wei-Ping Zhu; M.N.S. Swamy, "Real-Valued ESPRIT for two-dimensional DOA estimation of noncircular signals for acoustic vector sensor array," in *Circuits and*

Systems (ISCAS), 2015 IEEE International Symposium on , pp.2153-2156, 24-27 May 2015.

[12] Han Chen; Wei-Ping Zhu; M.N.S. Swamy, " Efficient 2-D DOA Estimation of Coherent Signals Using Two Parallel Uniform Linear Acoustic Vector-Sensor Subarrays," Submitted to *Circuits and Systems (ISCAS), 2016 IEEE International Symposium on* . (Under review)

[13] Arunkumar, K.P.; Anand, G.V., "Multiple source localization in shallow ocean using a uniform linear horizontal array of acoustic vector sensors," in Proc. of *TENCON 2007 - 2007 IEEE Region 10 Conference*, pp.1-4, Oct. 2007.

[14] Tam, P.K.; Wong, K.T., "CramÉr-Rao Bounds for Direction Finding by an Acoustic Vector Sensor Under Nonideal Gain-Phase Responses, Noncollocation, or Nonorthogonal Orientation," *IEEE Sensors Journal* , vol.9, no.8, pp.969-982, Aug. 2009.

[15] Abdi, A.; Huaihai Guo, "Signal Correlation Modeling in Acoustic Vector Sensor Arrays," *IEEE Transactions on Signal Processing*, vol.57, no.3, pp.892-903, March 2009.

[16] Hawkes, M.; Nehorai, Arye, "Wideband source localization using a distributed acoustic vector-sensor array," *IEEE Transactions on Signal Processing*, vol.51, no.6, pp.1479-1491, June 2003.

[17] Zou, Nan; Chia Chin Swee; Chew, B.A.L., "Vector Hydrophone Array Development and its Associated DOA Estimation Algorithms," in Proc. of *OCEANS 2006 - Asia Pacific*, pp.1-5, May 2007.

[18] Jin He, Zhong Liu, “Two-dimensional direction finding of acoustic sources by a vector sensor array using the propagator method,” *Signal Processing*, vol. 88, issue 10, pp. 2492-2499, October 2008.

[19] Pillai, S.U.; Kwon, B.H., "Forward/backward spatial smoothing techniques for coherent signal identification," *IEEE Transactions on Acoustics, Speech and Signal Processing*, vol.37, no.1, pp.8-15, Jan. 1989.

[20] Tie-Jun Shan; Wax, M.; Kailath, T., "On spatial smoothing for direction-of-arrival estimation of coherent signals," *IEEE Transactions on Acoustics, Speech and Signal Processing*, vol.33, no.4, pp.806-811, Aug 1985.

[21] Jian Li, "Improved angular resolution for spatial smoothing techniques," *IEEE Transactions on Signal Processing*, vol.40, no.12, pp.3078-3081, Dec 1992.

[22] Seenu S. Reddi, Alex B. Gershman, “An alternative approach to coherent source location problem,” *Signal Processing*, vol.59, issue 2, pp.221-233, June 1997.

[23] Dominic Grenier, Éloi Bossé, “A new spatial smoothing scheme for direction-of-arrivals of correlated sources,” *Signal Processing*, vol.54, issue 2, pp.153-160, October 1996.

[24] Petit, E.; Jourdain, G., "An efficient self-recovering adaptive algorithm for BPSK signals transmitted through underwater acoustic channels," in Proc. of *International Conference on Acoustics, Speech, and Signal Processing 1995 (ICASSP-95),* vol.5, pp.3159-3162, May 1995.

[25] Pascal Chargé, Yide Wang, Joseph Saillard, “A non-circular sources direction finding method using polynomial rooting,” *Signal Processing*, vol.81, issue 8, pp.1765-1770, August 2001.

[26] Haardt, M.; Römer, F., "Enhancements of unitary ESPRIT for non-circular sources," in Proc. of *IEEE International Conference on Acoustics, Speech, and Signal 2004 (ICASSP '04)*, vol.2, pp.ii-101-4, May 2004.

[27] Roy, R.; Kailath, T., "ESPRIT-estimation of signal parameters via rotational invariance techniques," *IEEE Transactions on Acoustics, Speech and Signal Processing*, vol.37, no.7, pp.984-995, Jul. 1989.

[28] Zoltowski, M.D.; Haardt, M.; Mathews, Cherian P., "Closed-form 2-D angle estimation with rectangular arrays in element space or beamspace via unitary ESPRIT," *IEEE Transactions on Signal Processing*, vol.44, no.2, pp.316-328, Feb. 1996.

[29] Jin He, Zhong Liu, “Efficient underwater two-dimensional coherent source localization with linear vector-hydrophone array,” *Signal Processing*, vol.89, issue 9, pp.1715-1722, Sept. 2009.

[30] P. Palanisamy, N. Kalyanasundaram, P.M. Swetha, “Two-dimensional DOA estimation of coherent signals using acoustic vector sensor array,” *Signal Processing*, vol.92, issue 1, pp.19-28, January 2012.

[31] Wax, M.; Ziskind, I., "Detection of the number of coherent signals by the MDL principle," *IEEE Transactions on Acoustics, Speech and Signal Processing*, vol.37, no.8, pp.1190-1196, Aug 1989.

[32] K. Minamisono, T. Shiokawa, “Prediction of the number of coherent signals for mobile communicatin systems using autoregressive modeling,” *Electronics and Communications in Japan (Part-1: Communications)*, vol.77, pp.71–79, 1994.

[33] K. Huang, Z. Huang, Y. Zhou, “Determining the number of coherent signal based on

covariance matrix transforming," *Signal Processing*, vol.19, pp.390–394, 2003.

[34] Tsuji, M.; Umebayashi, K.; Kamiya, Y.; Suzuki, Y., "A study on the accurate estimation of the number of weak coherent signals," in Proc. of *European Radar Conference 2009 (EuRAD 2009),* pp.234-237, Sept. 2009.

[35] Zhen, Jiaqi; Si, Xicai; Liu, Lutao, "Method for determining number of coherent signals in the presence of colored noise," *Journal of Systems Engineering and Electronics*, vol.21, no.1, pp.27-30, Feb. 2010.

[36] Viberg, M.; Ottersten, B.; Kailath, T., "Detection and estimation in sensor arrays using weighted subspace fitting," *IEEE Transactions on Signal Processing*, vol.39, no.11, pp.2436-2449, Nov 1991.

[37] Wax, M.; Kailath, T., "Detection of signals by information theoretic criteria," *IEEE Transactions on Acoustics, Speech and Signal Processing*, vol.33, no.2, pp.387-392, Apr 1985.

[38] Jingmin Xin; Nanning Zheng; Sano, A., "On-line detection of the number of narrowband signals with a uniform linear array," in Proc. of *16th European Signal Processing Conference,* pp.1-5, Aug. 2008.

[39] A.K. Seghouane, "Multivariate regression model selection from small samples using Kullback's symmetric divergence," *Signal Processing,* vol.86, pp.2074–2084,2006.

[40] Yuehua Wu; Kwok-Wai Tam, "On determination of the number of signals in spatially correlated noise," *IEEE Transactions on Signal Processing*, vol.46, no.11, pp.3023-3029, Nov 1998.

[41] Nehorai, Arye; Paldi, E., "Vector-sensor array processing for electromagnetic source localization," *IEEE Transactions on Signal Processing*, vol.42, no.2, pp.376-398, Feb 1994.

[42] Jingmin Xin and Sano, A., "Computationally efficient subspace-based method for direction-of-arrival estimation without eigendecomposition," IEEE Trans. on Signal Processing, vol.52, no.4, pp.876-893, Apr. 2004.

[43] Tayem, N.; Kwon, H.M., "L-shape 2-dimensional arrival angle estimation with propagator method," *IEEE Transactions on Antennas and Propagation*, vol.53, no.5, pp.1622-1630, May 2005.

[44] Kikuchi, S.; Tsuji, H.; Sano, A., "Pair-Matching Method for Estimating 2-D Angle of Arrival With a Cross-Correlation Matrix," *IEEE Antennas and Wireless Propagation Letters*,

vol.5, no.1, pp.35-40, Dec. 2006.

[45] Jian-Feng Gu, Ping Wei, Heng-Ming Tai, "2-D direction-of-arrival estimation of coherent signals using cross-correlation matrix," *Signal Processing*, vol.88, issue 1, pp.75-85, January 2008.

[46] B. Picinbono, "On circularity," *IEEE Transactions on Signal Processing*, 1994, 42(12): 3473- 3482